International Journal of Mass Spectrometry 277 (2008) 4–25

Contents lists available at ScienceDirect

International Journal of Mass Spectrometry

journal homepage: www.elsevier.com/locate/ijms

From isolated molecules through clusters and condensates to the building blocks of life
A short tribute to Prof. Eugen Illenberger's work in the field of negative ion chemistry

Ilko Bald[a], Judith Langer[b], Petra Tegeder[c], Oddur Ingólfsson[a,*]

[a] Department of Chemistry, University of Iceland, Science Institute, Dunhaga 3, 107 Reyklavík, Iceland
[b] Institut für Optik und Atomare Physik, Technische Universität Berlin, Hardenbergstr. 36, D-10623 Berlin, Germany
[c] Institut für Experimentalphysik, Freie Universität Berlin, Arnimallee 14, D-14195 Berlin, Germany

ARTICLE INFO

Article history:
Received 30 March 2008
Received in revised form 12 June 2008
Accepted 16 June 2008
Available online 26 June 2008

A short tribute to Prof. Eugen Illenberger's work in the field of negative ion chemistry.

Keywords:
Dissociative electron attachment
Electron stimulated desorption
Cluster anions
DNA nucleobases
Temperature dependency

ABSTRACT

Electron attachment processes in isolated molecules in the gas phase, in clusters and in molecules condensed on surfaces are reviewed, and a special section is dedicated to electron attachment to biologically relevant molecules. For isolated molecules in the gas phase the emphasis is on the comparison between direct dissociation from strongly repulsive σ^* states and the more indirect predissociation processes associated with the initial occupation of a π^* MO. These processes are discussed with regard to the temperature dependence of the dissociative electron attachment processes and with regard to its high bond selectivity. Specific examples of high bond and site selectivity at particular electron incident energies are discussed in terms of thermo-chemically controlled and state controlled selectivity of the dissociative electron attachment process. Different processes that are specific for electron attachment to molecules in clusters or condensed on surfaces are discussed for prototypical cases. These include suppression and enhancement of DEA channels, negative ion formation through "electron/exciton-complexes", scavenging processes, and low energy electron induced synthesis in thin molecular films and in clusters. Finally we discuss gas phase electron attachment to the DNA and RNA building blocks, i.e., the nucleobases, the sugar unit and the phosphate group. The relevance of these gas phase experiments to actual DNA damage such as single strand breaks is discussed and first gas phase electron attachment experiments on larger DNA units are discussed.

1. Introduction

It is a great honor and a pleasure for us to have the opportunity within the frame of this celebration issue of the IJMS to bring our best whishes to Prof. Eugen Illenberger on the occasion of his 65th birthday. And what could be more adequate than expressing these whishes in the form of a short tribute to his work in the field of negative ion chemistry. A field, in which Eugen is one of the leading capacities, a field he helped shaping with his contributions and a field where his input has had great influence on our knowledge and understanding. Moreover, besides being a very fruitful and disciplined scientist Eugen is also a great mentor, a friend to his students and supportive far beyond the duration of their studies. As his students we all have experienced these qualities and benefited from them greatly. For this we would also like to express our gratitude to Eugen on this special occasion.

In the year 1989 Eugen took a position as a Professor of Physical Chemistry at the Free University in Berlin where he has established one of the most active laboratories in the field of gas phase negative ion chemistry. Moreover, he has not limited his studies to negative ions in the gas phase but extended them *from isolated molecules through clusters and condensates to the building blocks of life*. In this short review we will attempt to offer the reader an impression of this journey and hopefully some insight into the multiplicity of Eugens work in the field of negative ion chemistry.

The formation and decay of negative ions is a field that has engaged great interest of physicists and physical chemists for several decades and considerable theoretical and experimental work has been dedicated to the subject (see, for example, refs. [1–3] and references therein). The first step in this process can be understood as the formation of a transient negative ion (TNI) through a vertical transition from the electronic ground state of the neutral molecule

* Corresponding author. Tel.: +354 525 4313; fax: +354 552 8911.
E-mail address: odduring@hi.is (O. Ingólfsson).

1387-3806/$ – see front matter © 2008 Elsevier B.V. All rights reserved.
doi:10.1016/j.ijms.2008.06.013

to the potential energy surface of the anion (Franck–Condon transition);

$$e^- + ABCD \rightarrow ABCD^{-\#}. \quad (1)$$

Here "#" signifies the anionic transient state, i.e., the excited molecular anion. This can be an electronically or a vibrationally excited TNI, however in the proceeding text we use "−#" to indicate a vibrationally excited TNI but "*−" for an electronically excited TNI.

In principle the only prerequisite for the existence of a bound state for the electron is that the ground state of the anion is energetically lower than the associated neutral precursor state, i.e., the molecule must possess a positive (adiabatic) electron affinity. However, as the TNI is formed through a vertical transition it must necessarily be in an excited state if the molecule in question possesses a positive electron affinity. The excitation energy; E, of the TNI, thus comprises the incident energy of the attached electron and the electron affinity of the molecule. At large distances, the interaction of the incoming electron with the target molecule is dominated by the attractive charge-induced dipole potential (V_α) but at short distances the repulsive centrifugal potential (V_l), originating from the angular momentum of the electron, becomes more important. The resulting interaction potential is the sum of the charge-induced dipole potential and the centrifugal potential; $V_{Eff} = V_\alpha + V_l$. Fig. 1 shows schematically the interaction potential for different angular momentum quantum numbers $l = 0$, 1 and 2. For $l \neq 0$ a centrifugal barrier is formed and the electron can be temporarily trapped within the effective potential. Referring to the shape of this interaction potential the TNI formed by this mechanism is termed *shape resonance* [4,5]. In the picture of molecular orbitals (MOs) the extra electron occupies a previously empty MO and if the electron configuration of the molecule is otherwise unchanged, i.e., no electronic excitation takes place, these resonances are also referred to as *single particle shape resonances*. Fig. 2 shows a schematic potential energy diagram for the total energy of a neutral molecule ABCD and two σ^* single particle shape resonances accessible through a vertical transition from the ground state of the neutral molecule. In this example the first resonance is associated with the lowest lying molecular orbital (LUMO) of the neutral with a highly localized σ^*(A–BCD) character the second is associated with a higher lying virtual σ^* MO located at the

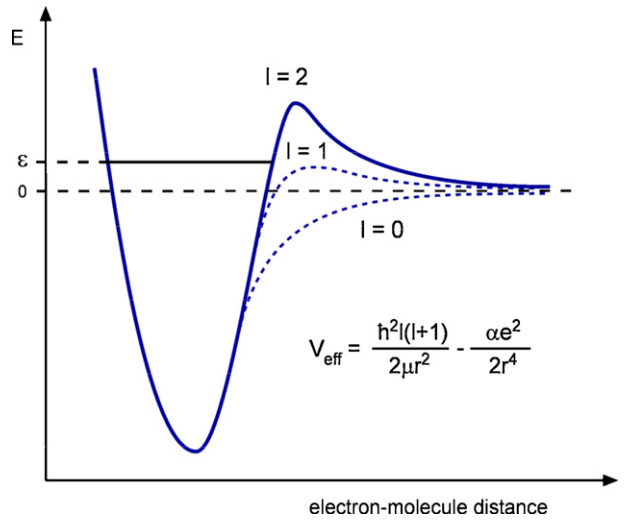

Fig. 1. Effective interaction potential for an electron approaching a neutral molecule. The effective potential is the sum of the charge-induced dipole potential and the centrifugal potential. When the angular momentum quantum number l is different from zero, a centrifugal barrier is formed and the electron can be temporarily trapped within the effective potential.

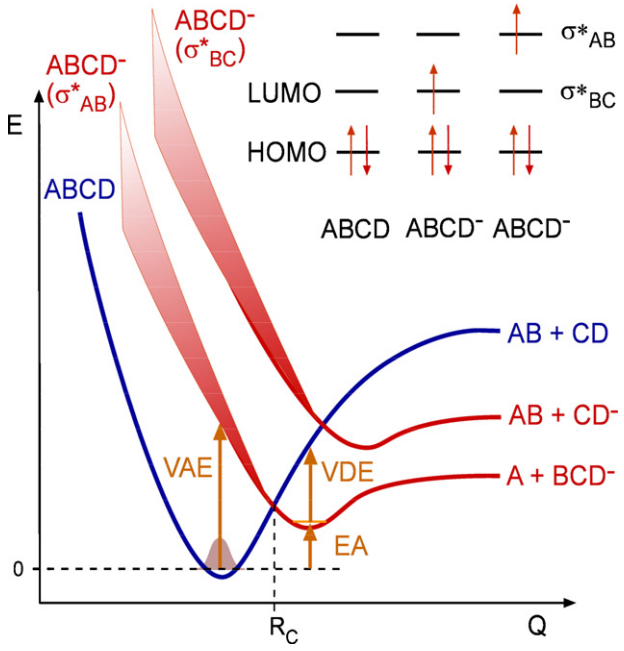

Fig. 2. Schematic potential energy diagram for the total energy of a neutral molecule ABCD and two σ^* shape resonances accessible through a vertical transition from the ground state of the neutral molecule.

AB–CD bond. The vertical electron attachment energy (VAE), which corresponds to the appearance energy of the resonance, the vertical detachment energy (VDE), which corresponds to the energy needed to re-eject the electron from the ground state of the negative ion and the adiabatic electron affinity; EA are signified in Fig. 2. Single particle shape resonances usually occur at electron energies <4 eV and typically have lifetimes in the range from 10^{-15} to 10^{-10} s [4,5]. Exceptionally long lifetimes, however, can be observed in highly symmetric polyatomic molecules where the Jahn–Teller distortion of the anion provides for efficient coupling between the different vibrational degrees of freedom and between the electronic and vibrational states involved [6,7]. This leads to a fast dissipation of the excess energy within the molecule, removing it from the coordinates relevant for the re-ejection of the electron or for dissociation of the molecule. Hence the lifetime of the molecular anion becomes extended through internal energy distribution. Examples of such stabilization effects through *intramolecular vibrational redistribution* (IVR) are the long lived (>10^{-5} s) low energy resonances in sulfur hexafluoride (SF_6) and hexafluoro benzene (C_6F_6) that are observed close to 0 eV electron energy (see, for example, refs. [1,3,8–10] and references cited therein).

If the energy of the incoming electron is large enough to induce an electron excitation in the neutral molecule, a resonance can form in which two electrons occupy a normally empty MO or MOs. A TNI formed in this way is called a *core excited* or a *two particle one hole* (2p–1h) resonance. If this TNI is energetically above the corresponding electronically excited neutral molecule the electron is bound by a centrifugal barrier like in the case of the shape resonances. The lifetime of this TNI is short and the resonance is referred to as a *core excited shape* or *core excited open channel resonance*. If on the other hand the TNI is energetically below the corresponding electronically excited state of the neutral molecule it cannot relax to that state by the simple ejection of the excess electron. In this case the TNI can only relax to a lower lying excited state or the ground state of the molecule through a two electron transition. This requires a considerable rearrangement of the electronic structure, which in turn extends the lifetime of the resonance with regard

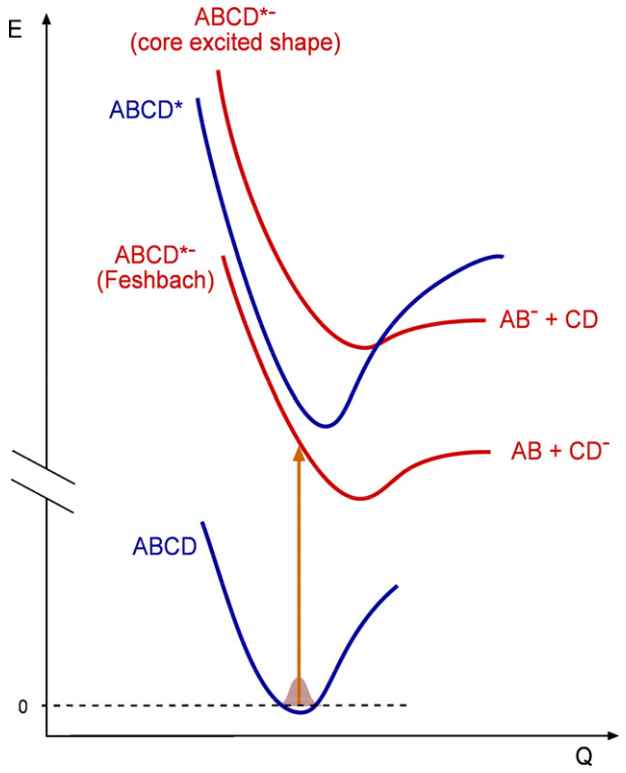

Fig. 3. Schematic potential energy diagram displaying the formation of a core excited open channel (shape) and a core excited closed channel (Feshbach) resonances within the same molecule. The resonances are depicted along the AB–CD dissoviative asymptote with AB being the fragment with the higher electron affinity. In this example both resonances are associated with the same excited state of the neutral and in the closed channel resonance both the excited electron and the excess electron are in the same MO, whereas in the open channel resonance these are depicted in different MOs.

to re-ejection of the electron. These resonances are referred to as *core excited Feshbach* or *core excited closed channel resonances*. Fig. 3 shows schematic potential energy curves illustrating the formation of the two different types of core excited resonances.

Feshbach resonances can also be formed at low energies if the vibrational levels of the TNI are below the corresponding states of the neutral [11,12]. These are called *vibrational Feshbach resonances* (VFR), a term which strictly refers to resonances that lie only a small amount of energy below the parent vibrational state (generally such that lowering the vibrational state by one quantum suffices to release the electron like in the case of HF [11,13]). However, here we also refer to VFRs for such resonances as the long-lived parent anions $SF_6^{-\#}$ and $C_6F_6^{-\#}$ (see above) where effective intramolecular energy distribution delays the re-ejection of the electron. VFRs are also observed from so-called *dipole-bound states* (DB) [14–16]. The prerequisite for the existence of a DB state is a high polarizability and a large dipole moment (>2.5 D). In this case the electron is bound by attractive long-range charge–dipole interaction and resides in a diffuse Rydberg-type orbital as observed, for example, in N_2O [17], ethylene carbonate [18] and uracil [19].

Irrespective of the mechanism leading to the formation of a TNI, under single collision conditions it can only relax by either ejecting the electron again; *autodetachment* (AD), through dissociation; *dissociative electron attachment* (DEA) or by energy release through light emission; *radiative relaxation*. Radiative relaxation is a process which proceeds on a much longer timescale compared to the relaxation through dissociation or re-ejection of the electron and will not be considered here. Autodetachment and dissociative electron attachment on the other hand are often operative on comparable timescales and the branching ratio between the two channels will mainly depend on which of the both processes is the faster one.

At very low electron energies the Wigner threshold law [20] describes the energy dependence of the "likelihood" of a two particle capture process in terms of the attachment cross section (σ_0) as:

$$\sigma_0(E, l) \sim E^{l-1/2} \quad (E \to 0) \tag{2}$$

For $l = 0$ (s-wave attachment) one would therefore expect an $E^{-1/2}$ dependence for the electron attachment cross section close to threshold. For p-wave attachment, on the other hand, where $l = 1$, the energy dependence is predicted to be $E^{1/2}$. Hence, due to the prerequisite of constructive interference for electron capture, the energy dependence of the cross section close to threshold is highly dependent on the symmetry of the anionic state [21]. In most cases the s-wave component governs the threshold behavior in electron attachment, even in cases such as C_{60} where s-wave attachment to the ground state is not expected to be operative [22,23]. P-wave attachment has been demonstrated in the case of Cl_2 [24] and very recently also for F_2 [25].

The electron attachment cross section is closely related to the attachment rate, i.e., the rate constant (k) for reaction (1). This can be fairly well described as the product of the mean electron velocity ($\bar{v}$) and the attachment cross section averaged over the relevant incident electron energies ($\bar{\sigma}$); $k = \bar{\sigma}\bar{v}$ [26,27]. Correspondingly the DEA cross section; σ_{DEA}, is the product of the attachment cross section; σ_0, and the dissociation probability P_{diss}.

$$\sigma_{DEA} = \sigma_0 P_{diss}. \tag{3}$$

Here P_{diss} expresses the probability of the TNI to reach the crossing point of the potential energy curves (marked R_C in Figs. 2 and 4) before the electron is re-ejected. Thus, this probability can be calculated from the autodetachment lifetime; τ_{AD} and the time it takes the TNI to dissociate τ_{DEA}:

$$\sigma_{DEA} = \sigma_0 \, e^{-\tau_{DEA}/\tau_{AD}}. \tag{4}$$

This is visualized in Fig. 4 in the simplified picture of a two-dimensional potential energy diagram. The autodetachment-lifetime τ_{AD} is related to the energy width Γ of the transient negative ion state according to the Heisenberg uncertainty principle. The dissociation lifetime can be calculated from the radial

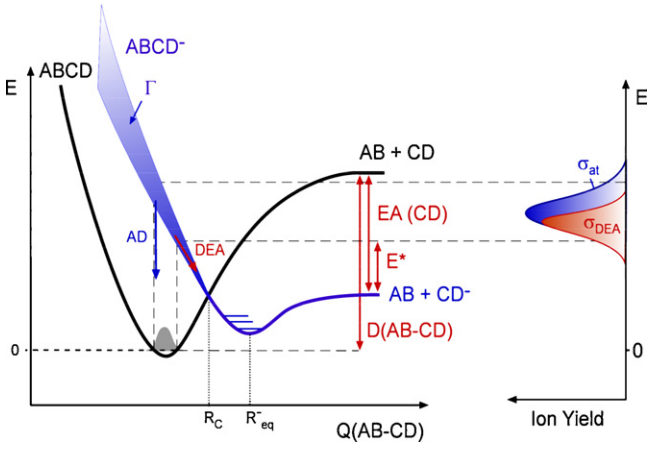

Fig. 4. Simplified two-dimensional potential energy diagram illustrating the formation of a transient negative ion. Autodetachment of the extra electron is possible until the crossing point R_C of the anionic and the neutral potential energy curve is reached. The ion yield shown on the right hand side reflects the initial Franck–Condon transition.

velocity $v(R')$ between the forming fragments according to:

$$\tau_{DEA} = \int_{R}^{R_c} \frac{dR'}{v(R')}. \quad (5)$$

Here R is the bond distance from where the electronic transition takes place and R_C is the crossing point. In Fig. 4 the TNI is formed through a vertical transition within the Frank–Condon region and then relaxes to reach its geometrical equilibrium R_{eq}^{-}. However, until the crossing point R_C is reached, autodetachment is still possible. In Fig. 4 the autodetachment lifetime is signified through the width of the resonance, which decreases at lower transition energies. When the bond relevant to the DEA process is elongated beyond R_C, autodetachment is not longer possible and the molecule is bound to dissociate. In a first approximation the ion yield curve reflects the transition probability within the Frank–Condon region; however, the position and the shape of the ion yield can also be strongly influenced by the autodetachment lifetime. Furthermore, if the anionic curve has a minimum, the parent ion $ABCD^-$ may be observed, given that the excess energy can be efficiently redistributed within the vibrational degrees of freedom of the molecule. However, in a simplified picture, the ion yield can be seen as a reflection of the initial Frank–Condon transition. This so called *reflection principle* [2,28,29] is shown on the right side of Fig. 4.

If a molecule is comparatively simple and the incident energy of the electron is low, DEA can often be fairly accurately described within the framework of a diatomic dissociation along the dissociative asymptote of a repulsive state leading to the formation of a negatively charged fragment and its radical counterpart;

$$ABCD^{-\#} \rightarrow AB + CD^{-}. \quad (6)$$

In more complex polyatomic molecules the excess energy can be distributed among a large number of vibrational degrees of freedom and the lifetime of the TNI is extended. As a consequence the DEA process can be complex and even involve considerable rearrangement within the molecule;

$$ABCD^{-\#} \rightarrow AC + BD^{-}. \quad (7)$$

Furthermore, the initial dissociation process can leave the fragments with appreciable amount of internal energy, which in turn can lead to further dissociation on a metastable (>10^{-6} s) time scale

$$ABCD^{-\#} \rightarrow AB^{(\#)} + CD^{-(\#)} \quad (8)$$

$$CD^{-(\#)} \rightarrow C + D^{-}. \quad (9)$$

In a molecular aggregate (cluster), as compared to isolated molecules in the gas phase, the situation changes considerably [3,30–32]. For one thing the formation of a TNI does not necessarily involve only one molecule within the cluster as the *de Broglie* wavelength (λ_D) of the electrons in the energy range under consideration is on the order of the intermolecular distance within the cluster (e.g., λ_D for a 1 eV electron is 1.2 nm). In addition, in larger clusters, bulk liquids and also in adsorbates of polar molecules such as water or ammonia, electrons may be trapped by the collective field of the oriented dipoles [33–36].

However, even if we consider the electron attachment process in a cluster as the interaction of the incoming electron with a *single* molecule within the cluster, the surrounding molecules still have a significant influence on the formation and the decay of the TNI. In the formation process the most important effects are (i) the polarization interaction of the neutral precursor and the TNI with the surrounding molecules and (ii) the energy loss of the incoming electrons through inelastic scattering from other molecules within the cluster prior to attachment. The former effect is depicted in Fig. 5 for net stabilization of both the molecular precursor and the TNI. The

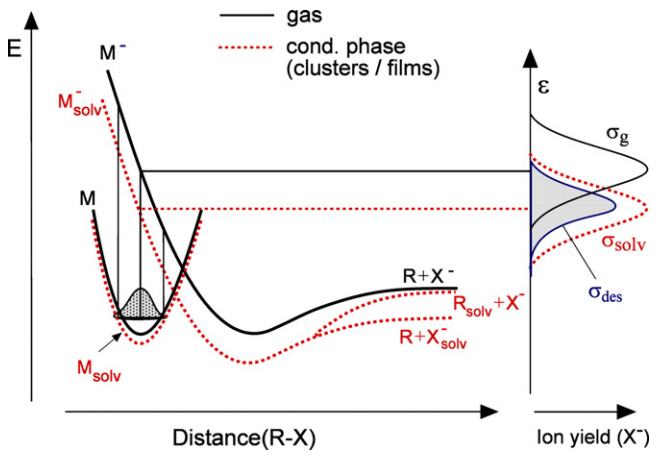

Fig. 5. Stabilization of the neutral molecule and the TNI in a condensed medium compared to the isolated molecule in the gas phase. The TNI is better stabilized than the neutral precursor due to the stronger polarization of the environment in the presence of a negative charge. On the right hand side the cross section for the X^- formation in the gas phase; σ_g, and for the condensed phase; σ_{solv}, is shown. For clarity the shift of the neutral potential energy curve is neglected in the ion yield curves. In addition the shift of the desorption cross section; σ_{des} is shown.

schematic potential energy curves are shown for the isolated neutral molecule and the corresponding negative ion in the gas phase compared to the potential energy curves in a cluster or condensates (signified by the subscript "solv"). The attractive polarization interaction can be considered as to be composed of two components; the fast electron polarization that takes place on the same time scale as the attachment process itself and the stabilization through the reorientation of the surrounding molecules which occurs on a much slower timescale (10^{-12} to 10^{-10} s). Due to the stronger polarization of the environment in the presence of a negative charge the result is a net stabilization of the TNI relative to the neutral precursor. This applies for the anion in its electronic ground state and due to the higher polarizability of the electronic excited states this stabilization effect is usually stronger in the case of core excited resonances. Largely, the same picture applies for molecules condensed in molecular films or at surfaces as will be discussed here below.

The effect of inelastic scattering processes on the formation of the TNI as it appears in the ion yield curves from molecular clusters is often not less important. The initial step in this process can be understood as the formation of a short-lived core excited open channel resonance. The resonance then decays through autodetachment, but leaves the neutral molecule in an excited state. Hence the electron loses most of its energy in an inelastic scattering event within the cluster. The electron is typically slowed down to around 0 eV after the scattering event and can thus be captured by another molecule through a low lying single particle resonance. This resonance is detectable by conventional mass spectrometric methods if it has sufficient lifetime with respect to autodetachment to be either stabilized through energy dissipation or to dissociate to form a stable negative ion fragment. In both cases this low lying single particle resonance appears in the ion yield curves "*blue shifted*" by the excitation energy left in the neutral molecule through the initial inelastic scattering process. If the initial scattering center and the scavenger are the same kind of molecules the process is referred to as *self-scavenging*. If the molecules are of different kind, the process is referred to as *auto-scavenging* (an explicit example of *auto-scavenging* processes (C_6F_5Cl/N_2) is given in supplementary material to this article). The electron can also slow down through non-resonant inelastic processes within the cluster, however these are much less efficient processes and do not appear as resonant features.

Beside the influences on the formation of the TNI, the cluster environment can also strongly influence its decay probability. In a cluster the intermolecular collision rate is on the same timescale as the vibrational frequencies, hence the immediate geometrical relaxation of the TNI upon formation is directly coupled to a fast and effective relaxation mechanism leading to dissipation of the vibrational fraction of its excess energy $E^{\#}$ within the cluster. This results in stabilization of the TNI with respect to dissociation as well as autodetachment and the excess energy is carried away through evaporation of a part or the entire cluster. The process is therefore often referred to as *evaporative attachment* [3,31,37].

In general the same processes that are operative in clusters can also play a significant role in adsorbed or condensed molecules [3,32,38–40]. However, the ion yield curves from electron stimulated desorption (ESD) from surfaces only show the ionic fragments that are desorbed. Therefore, many processes that result from electron attachment to condensed molecules are not directly observable by means of conventional mass spectrometric analysis.

If we consider electron attachment to molecules in the condensed phase, the fate of the TNI formed at or near a surface or in a molecular film can principally be described through the following reactions (the subscript (ad) denotes the particle at the surface);

$$e^- + M_{ad} \rightarrow M^{-\#}{}_{ad}$$

$$\rightarrow M^-_{ad} \quad (10)$$

$$\rightarrow R_{ad} + X_{ad}^- \quad (11)$$

$$\rightarrow R + X_{ad}^- \quad (12)$$

$$\rightarrow R_{ad} + X^- \quad (13)$$

The branching ratio between the channels (11)–(13) depends on the orientation of the molecules at the surface, since a fragment facing in the direction of the surface has the least escape probability and a fragment pointing away from the surface has the highest escape probability. More important for our discussion here is the fact that in reactions (12) and (13) the desorbing fragment has to overcome the polarization barrier to leave the surface. This is depicted on the right hand side of Fig. 5 where the ion yield curves as they would result from the reflection principle for an isolated molecule (σ_g) and a molecule solvated in a condensate or adsorbed at the surface (σ_{solv}) are compared to the fraction of the fragment ions that have sufficient energy to overcome the polarization force and escape the surface (σ_{des}). This makes the branching ratios highly dependent on the energetics of the underlying DEA process, i.e., the kinetic energy release to the fragments and the strength of their polarization interaction with the surface and/or surrounding molecules. The DEA channels listed above are therefore energetically less favourable in order of their appearance (11)–(13), making the only channel that is observable with conventional mass spectrometry the energetically least favourable (reaction (13)).

In addition to the DEA processes the TNI may also relax through energy transfer to the surface or energy dissipation within the condensate (reaction (10)). Comparable to evaporative attachment in clusters this may result in the formation of the thermodynamically stable molecular ion $M_{ad}{}^-$, but now trapped at the surface or within the condensate. This process and the DEA reactions (11) and (12) will contribute to charging of the film, which again influences the energy dependence of low energy electron transmission through the film. Thus the resonant formation of molecular anions as well as fragment ions that do not escape the attractive polarization force can be probed by means of electron transmission [41–43]. In addition to ESD and electron transmission spectroscopy also infrared-reflection-absorption-spectroscopy (IRAS) was applied in Eugen's group to study electron induced reactions in thin molecular films [44].

In this review we present examples of the different types of resonances and selected case studies on their energy and temperature dependence. We present general considerations on the high selectivity of DEA processes with regard to bond cleavage and how this may be used to control chemical reactions. In this context we present selected case studies on the influence of the environment in clusters and in condensates. Finally we dedicate a part of this review to Eugen's work in the field of low energy electron interaction with biological relevant molecules, a field in which Eugen has been very active in recent years.

2. Experimental considerations

2.1. Isolated molecules, clusters and condensates

For detailed description of the apparatuses from Eugen's group that were used for the studies described in this review we refer the reader to the references [2,45,46] for the gas phase studies on isolated molecules, to the references [2,3,47] for studies on molecules in clusters and to the references [3,43,44,48] for studies on molecules condensed on surfaces. Also a more detailed description of the Berlin experimental setups can be found in the supplementary material to this review.

In brief, the gas phase experiments described here are all crossed beam studies where an effusive or a cluster beam is crossed with a beam of monochromatic low energy electrons generated by a trochoidal electron monochromator (TEM) [49]. The anionic products are extracted by a weak draw out field (<1 V cm^{-1}) and analyzed by a quadrupole mass spectrometer (QMS). Time-of-flight (ToF) measurements can be used to determine the kinetic energy release in the dissociation processes of isolated molecules. Details of this QMS-ToF measurement technique are given in the references [3,31,50]. The experimental setup to study isolated molecules in the gas phase is shown in Fig. 6. In this setup gas phase samples are entered into the reaction zone through an effusive inlet, liq-

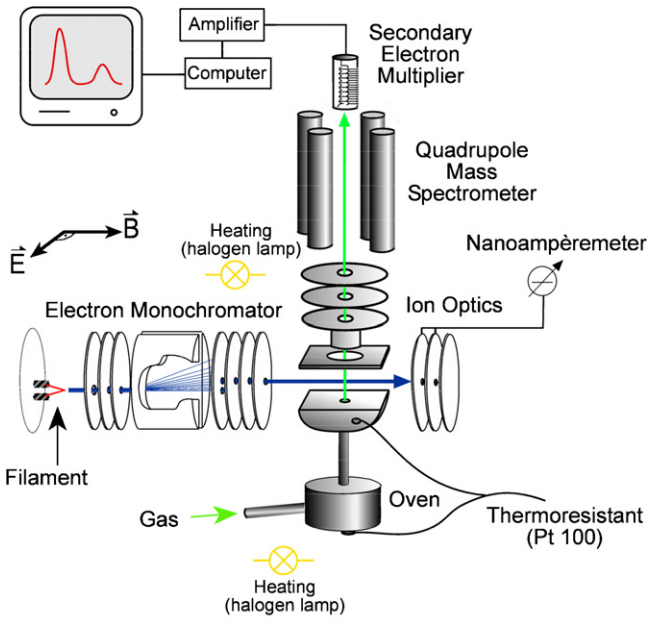

Fig. 6. Scheme of the experimental setup to study dissociative electron attachment to gas phase molecules.

uids are carried into the chamber in a saturated inert gas stream and solid samples are sublimed through a capillary from a heated vessel. The effusive gas inlet also passes through the vessel and can thus be heated up to 850 K, allowing for temperature dependent studies. The experimental setup to study clusters is essentially the same except that the cluster beam is generated from a continuous supersonic expansion and enters the reaction zone through a skimmer that separates the expansion chamber from the reaction chamber. The ion yield is typically recorded as a function of the electron energy in the range from 0 to 15 eV. The maximum formation probability of SF_6^- at 0 eV is used to establish the zero point of the energy scale and the full width at half maximum (FWHM) of the same resonance is used to determine the energy resolution which is typically in the range from 80 to 150 meV.

To study electron attachment to molecules at surfaces or within condensates the target molecules are condensed on a cryogenically cooled (≈30 K) monocrystalline gold (or platinum) substrate by exposing it to a volumetrically calibrated gas quantity. The metal substrate is mounted on a manipulator and can thus be rotated at any desirable angle relative to the TEM and the QMS which are arranged perpendicular to each other. The condensed molecules are exposed to the electron beam which is typically scanned from about 0–15 eV and ion desorption yields are measured. Also electron transmission spectra can be recorded with this setup by monitoring the current at the metal substrate. The electron energy is calibrated by the onset of the electron transmission to the substrate (0 eV, vacuum level) and the resolution of the electron beam is determined from the steepness of the onset and is typically around 0.2 eV at currents of about 30 nA (for a more detailed description see ref. [3]). In order to study electron induced reactions in thin molecular films this experimental setup was also extended to measure adsorbate vibrations by means of infrared-reflection-absorption-spectroscopy [44].

2.2. Laser induced acoustic desorption

The main drawback of the setup for studying isolated molecules in the gas phase is when it comes to the evaporation of large molecules through sublimation as many of these molecules decompose close to their sublimation temperature. This is especially true for larger biologically relevant molecules and even dipeptides, nucleosides and nucleotides cannot be brought into the gas phase by thermal evaporation without decomposition. Recently this problem was addressed in Eugen's group by the introduction of a new electron attachment spectrometer specifically designed to study thermally instable involatile molecules in the gas phase [51,52]. The principle of this electron attachment spectrometer is the same as described above, except that involatile molecules are transferred into the gas phase by laser induced acoustic desorption (LIAD) [53,54]. Fig. 7 shows schematically the desorption process in LIAD. The sample is deposited on a thin Ti-foil (12.7 μm) and faces towards the QMS. A pulsed beam from a Nd–YAG laser at 532 nm is focused on the back of the foil. The high energy density and the short duration of the pulse (3 mJ/pulse, width = 2–6 ns) causes the surface to heat up very rapidly [53]. The rapid, local heating generates an acoustic wave that traverses the metal foil and is reflected from the opposite metal/vacuum interface (Fig. 7). This results in a distortion of the "*dark side*" of the surface which in turn causes desorption of molecules. The energy transferred to the desorbing molecules is not more than a few kcal mol^{-1} which is not sufficient to fragment or ionize the sample molecules [55]. Hence, LIAD offers an ideal way to study fragile involatile molecules in the gas phase [54,55].

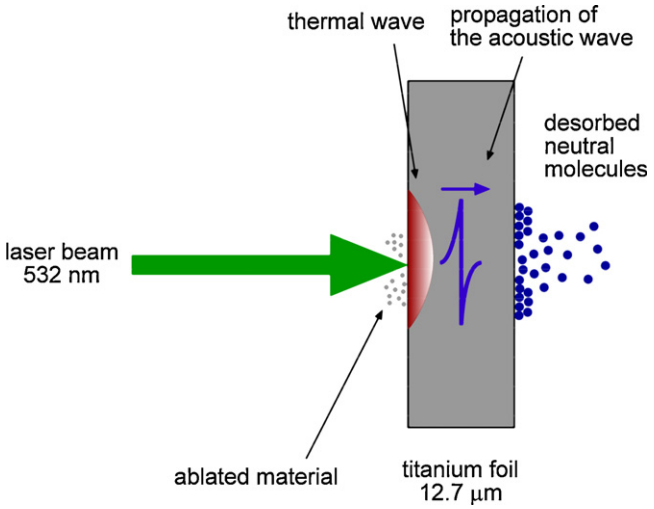

Fig. 7. Scheme of the desorption process in LIAD. A short laser pulse generates a shock wave that propagates through the metal foil to the opposite side, on which the sample is deposited. The molecules are desorbed without ionization and fragmentation (adapted from ref. [158]).

3. Results and discussion

3.1. Electron attachment to isolated molecules in the gas phase

Electron attachment to molecules in the gas phase, clusters and condensed phase has been studied on a multiplicity of molecular systems in the last decades. The bulk of these systems are halogenated compounds and the studies were originally triggered by their dielectric properties and use as gas phase insulators [1,56], their role in plasma etching [57] and in the earth's atmosphere [58]. In the meantime a considerable number of non-halogenated compounds have also been studied and in recent years the attention has moved towards biologically relevant molecules [59]. Furthermore, reactions of molecules with low energy electrons, i.e., electrons with energy in the range from 0 to 15 eV, are often highly selective and very effective. This selectivity can in many cases be accurately controlled by simple variation of the electrons kinetic energy within few electron volts. Thus low energy electrons might offer the means to accurately control chemical reactions at the molecular level with high efficiency and relatively simple instrumentation.

In this section we will focus on the selectivity of low energy electron attachment processes within isolated molecules in the gas phase. We will first review some prototypical cases of vibrational predissociation and compare those to direct dissociation along strongly repulsive potential energy surfaces. We will then discuss the influence of the temperature on DEA processes. Finally we present examples where high selectivity is observed in dissociative electron attachment and we discuss the origin of this selectivity.

3.1.1. Vibrational predissociation processes versus direct dissociation

In many cases DEA can be understood in a quasi-diatomic picture as a direct dissociation along a repulsive σ^* state. However, it is probably more common that considerable energy redistribution and even rearrangements within the molecules take place prior to or during the dissociation process. Such processes are referred to as vibrational predissociation processes and are usually associated with an initial occupation of a low lying π^* MO. The initially occupied π^* MO couples with a repulsive σ^* state leading to dissociation along the repulsive σ^* coordinate. A fairly simple example of such vibrational predissociation processes are observed in pro-

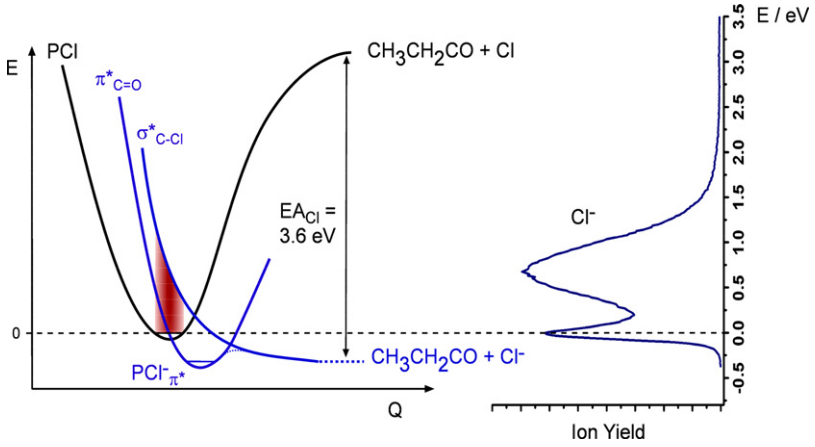

Fig. 8. Schematic potential energy diagram for the neutral and anionic ground state of $CH_3CH_2C(O)Cl$ along with the energetically higher lying σ^*(C–Cl) state. The Cl^- yield is displayed on the right as a reflection of the transition probability in the Franck–Condon region (adapted from ref. [60]).

pionyl chloride ($CH_3CH_2C(O)Cl$). Moreover, in this compound the predissociation process is observed on the same fragment as the direct dissociation [60]. Fig. 8 shows schematic potential energy curves for the neutral and anionic ground state of $CH_3CH_2C(O)Cl$ along with the energetically higher lying σ^*(C–Cl) state. The Cl^- yield is displayed on the right as a reflection of the transition probability in the Franck–Condon region. In the ion yield curve Cl^- is observed through a narrow contribution at 0 eV and a broader contribution shifted to higher energy. The Cl^- yield through the narrow resonance at 0 eV is interpreted as the result of a predissociation process involving an initial occupation of the π^*(C=O) LUMO with initial vibrational excitation of the C=O bond. The broader contribution centred around 0.7 eV on the other hand is interpreted to be due to direct dissociation along the repulsive σ^*(C–Cl) state. The higher energy contribution simply mirrors the transition probability but the shape and narrowness of the low energy resonance is again probably dominated by the autodetachment lifetime as seen through the corresponding experimental window. Both signals are comparable in intensity which is attributed to the inverse energy dependence of the cross section compensating for the higher efficiency of the direct dissociation process.

An interesting situation in DEA is also faced when strongly electronegative substituents are bound by a σ-bond to a more extensive, comparatively electronegative π-system. Like in the case of propionyl chloride the lowest lying resonance in such systems is commonly associated with an occupation of a π^* LUMO but the DEA products result from a cleavage of the σ-bond. The most comprehensive systematic study on such systems is probably the study on the mono-halogenated pentafluorobenzenes C_6F_6–X (X = F, Cl, Br, I) conducted in Eugen's lab in the mid 1990s [3,61]. These systems are particularly well suited to study the thermodynamics of the dissociation processes as well as the influence of the conjugation of the substituents with the ring system. First, they all form TNIs close to 0 eV, second, the electron affinity of C_6F_6X increases in the order F, Cl, Br and I due to their σ-acceptor/π-donor properties [62] and third, the reaction enthalpy (ΔH_0) for the formation of X^- gradually changes from being endothermic by 1.5 eV for X = F to being exothermic by 0.2 eV for X = I [3,61]. In all these cases the low energy resonance is understood as the formation of a vibrational Feshbach resonance through the occupation of a low lying π^* MO of the aromatic ring. The out-of-plane distortion through the occupation of the π^* MO induces strong coupling with the σ^*(C–X) MO, which again leads to an inherent competition between the survival of the TNI and the dissociation of the C–X bond to form either $C_6F_5^-$ or X^-. Hence the dissociation must be understood as a *vibrational predissociation* process. The branching ratios of the M^-, X^- and $C_6F_5^-$ formation below 1 eV are approximately 1:0:0, 100:400:1, 1:25:5 and 0:1:20 for X = F, Cl, Br and I, respectively. The dissociation dynamics of these systems and the branching ratios between the different channels can largely be understood in terms of the thermodynamic thresholds for the individual processes [3,61]. Very recently also the compounds C_6F_5CN and $C_6F_5NO_2$ [63], and also C_6F_5NCO and $C_6F_5CH_2CN$ [64] were studied with respect to their reactivity towards low energy electron attachment. In contrast to the pentafluoro halobenzenes, these systems have two strongly electronegative π-systems connected via a σ-bond. Pentafluoro phenylacetonitrile (C_6F_5–CH_2–CN) is an exception as a CH_2 group serves as a spacer between the two π-systems. Comparable to the pentafluoro halobenzenes one expects resonances in these compounds involving the lowest π^* orbitals of the aromatic ring, but also the lowest lying π^* orbitals of the substituent. In fact the most intense signal in all these compounds is from the molecular ion (M^-) through a narrow resonance close to 0 eV. An exception is pentafluoronitrobenzene (C_6F_5-NO_2) where no stable parent ion is observed. Fig. 9 shows the ion yield curves for the complementary ions $C_6F_5^-$ and NO_2^- from $C_6F_5NO_2$ (Fig. 9a and b) and $C_6F_5^-$ and CN^- from C_6F_5CN (Fig. 9c and d), respectively [63]. For $C_6F_5NO_2$ (Fig. 9a and b) both fragments have virtually identical resonance profiles with a low energy resonance peaking at 0.17 eV and a higher energy resonance at 3.4 eV. However, the branching ratio between the fragments formed through the low energy resonance is about 1:250 in favour of the larger fragment $C_6F_5^-$. At the HF/6-31G* level of theory the vertical attachment energy (VAE) of the lowest lying MO is negative and the LUMO+1 possesses 4 nodes on the ring system, similar to the e_{2u} MO in the first benzene resonance. The LUMO+2 on the other hand, whose VAE is calculated at HF/6-31G* level of theory to be 0.58 eV is found to have an appreciable σ^*(C–NO_2) character [63]. Correspondingly it is suggested that the low energy resonance that predominantly leads to cleavage of the C–NO_2 bond in $C_6F_5NO_2$ is associated with occupation of the LUMO+2. The higher energy resonance at 3.4 eV, however, correlates well with an optical band at 3.72 eV due to an $n_O \rightarrow \pi^*(NO_2)$ transition [65] and is thus interpreted as a core excited resonance with two electrons in a previously empty $\pi^*(NO_2)$ orbital and a hole in an n_O orbital. The 3.4 eV resonance also leads to the formation of F^-, $C_5F_5^-$, $C_5F_4^-$ and $C_3F_3^-$ with appreciable intensities.

In C_6F_5CN the formation of the molecular ion through a narrow resonance at 0 eV is by far the most intense signal, exceeding the fragmentation reactions shown in Fig. 9c and d by a factor of 1000. The complementary fragments $C_6F_5^-$ and CN^- shown in

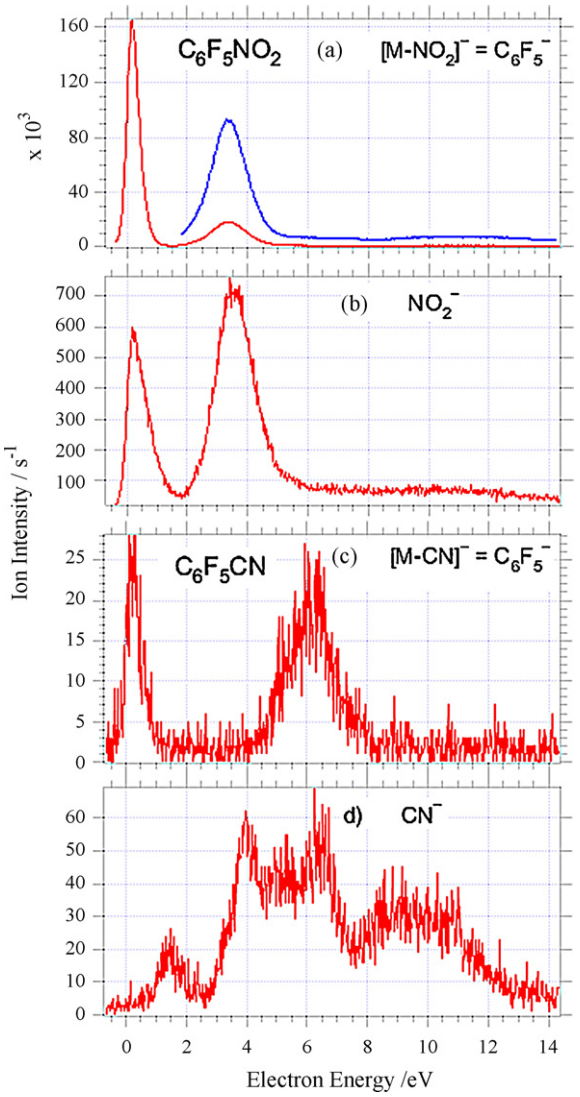

Fig. 9. Ion yield curves for the complementary ions; (a) $C_6F_5^-$ and (b) NO_2^- generated by DEA to $C_6F_5NO_2$, and (c) $C_6F_5^-$ and (d) CN^- generated from C_6F_5CN, respectively [63].

Fig. 9c and d, respectively, appear only with low intensities and no CN^- is observed through the low energy resonance close to 0 eV. An inspection of the lowest lying MOs as calculated at the HF/6-31G* level shows that the first accessible virtual MO is located on the aromatic ring and has no obvious σ^* component [64]. Hence the single electron occupation of this MO is similar to the lowest lying ($^2E_{2u}$) resonance in benzene [65]. The lifetime of the TNI is extended by effective vibrational energy redistribution and the observed width is essentially controlled by the autodetachment lifetime. The very weak $C_6F_5^-$ signal that peaks close to 0.2 eV is surprising as the energy threshold for the $C_6F_5^-$ formation is estimated to be close to 2 eV [63]. Low intensity signals close to 0 eV are however relatively often observed for processes with considerably higher threshold and are often associated with hot band transitions [66,67] or so called trojan horse ionization[68]. The ion $C_6F_5^-$ is also formed through a core excited resonance close to 6 eV which is most likely associated with an excitation within the aromatic system. It is not obvious from the ion yield if this resonance also leads to CN^- formation, but CN^- is mainly formed through relatively narrow resonances close to 1.5, 4 and 6.5 eV. The 1.5 and 4 eV resonances are specific to the CN^- fragment and correlate well with

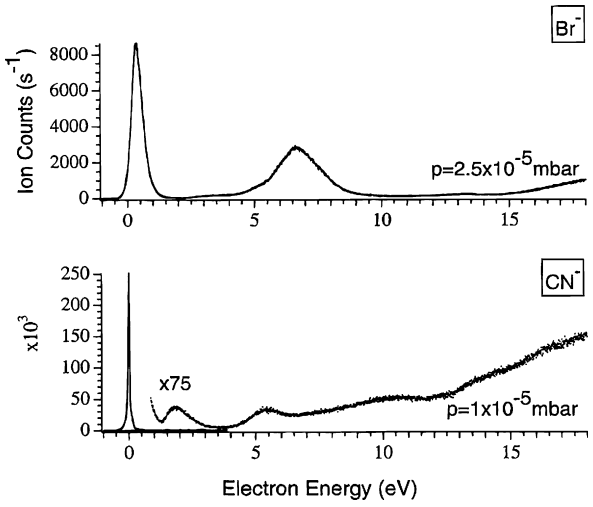

Fig. 10. Ion yields for the Br^- and CN^- formation from electron attachment to BrCN under single collision conditions. Reproduced from Brüning et al. [71] by permission of the American Chemical Society (Copyright 1996).

the $CN^*(^2\Pi)$ state at 1.15 eV [69], with the $CN^{*-}(^2\Pi)$ at 2.07 eV [70] and the $CN^*(^2\Sigma)$ state at 3.2 eV [69], respectively.

At large C_6F_5NCO and $C_6F_5CH_2CN$ show the same behaviour as C_6F_5CN. However, $C_6F_5CH_2CN$ shows an additional strong CN^- contribution centred around 0.78 eV which is tentatively assigned to an initial occupation of a $\pi^*(CN)$ MO [64]. The excess energy which is initially located in the CN stretch mode is then transferred to the relevant CH_2–CN coordinate.

The simplest molecules where an electronegative π-system is connected directly to a strongly electronegative substituent via a σ-bond are the cyanogen halides ClCN, BrCN and ICN. [71]. Fig. 10 shows the ion yields for the CN^- and Br^- formation from electron attachment to BrCN under single collision conditions. The corresponding spectra for ClCN are shown in the next section. In both cases, though more apparent on BrCN, CN^- is formed through a narrow resonance at 0 eV and the complementary halogen ion appears through a considerably broader feature slightly shifted to higher energy. *Ab initio* calculations [71] predict two low lying anionic states for BrCN from which one has a predominating σ^*(Br–CN) character the other a predominating π^*(CN) character. In line with the calculations the narrow resonance at 0 eV is interpreted as to be associated with the low lying π^*(CN) MO leading to the initial formation of $BrCN^-(^2\Pi)$ with the excess energy in the CN stretch vibration. The width as observed in the ion yield partly reflects the narrowness of the underlying transition but is probably mainly defined by the energy dependence of the autodetachment lifetime of the ion. The Br^- formation on the other hand proceeds via a direct dissociation from a single particle shape resonance involving the strongly repulsive σ^*(Br–CN) state, i.e., the initial formation of $BrCN^-(^2\Sigma)$. Hence here we have a case where in the same energy range vibrational predissociation leads to the formation of one fragment and the direct dissociation to another.

3.1.2. Temperature dependence in dissociative electron attachment

It has been shown in a number of studies in the past that the ion yield resulting from DEA may change considerably with temperature [1,66,72]. This is mainly due to the fact that the formation of the TNI is coupled to vibrational excitation. Thus, the occupation of the vibrational states of the neutral molecule can have strong effects on their fragmentation. How this influence manifests itself

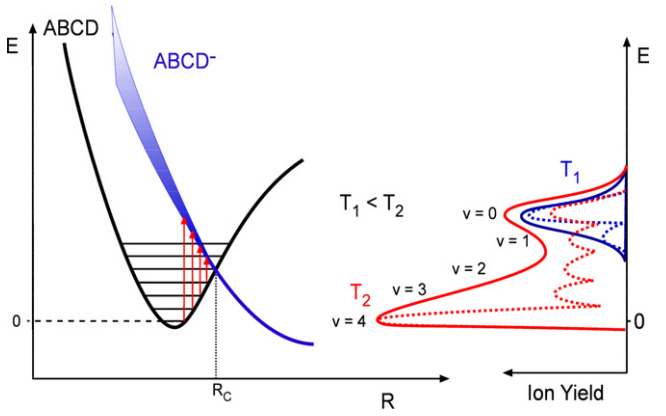

Fig. 11. Schematic potential energy curves for the neutral ground state; ABCD, and a strongly repulsive anionic state; $ABCD^-$. The vertical lines indicate the transition to the anionic state at threshold for the vibrational levels $v = 0$–4. On the right side the resulting DEA cross sections are shown schematically for two different temperatures for the same vibrational levels.

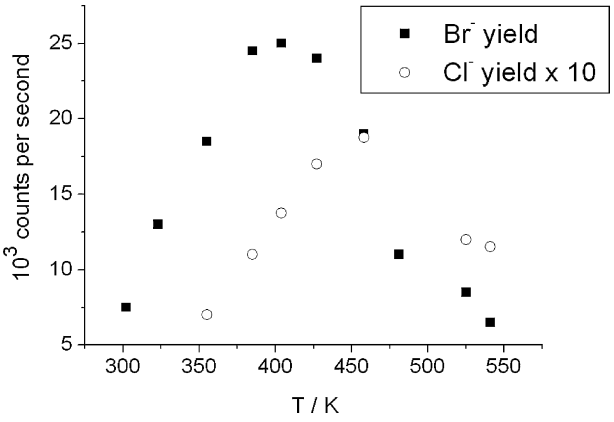

Fig. 12. Temperature dependence of the Br^- and Cl^- yield generated by DEA to 1,4-C_6H_4BrCl in the temperature range from room temperature to 550 K [74]. Both ion yields first increase and have a maximum close to 400 and 460 K, respectively. The ion yield then decreases at higher temperatures due to a depopulation of vibrational levels from which dissociation is still possible.

in the ion yield curves of the individual fragments is complex and depends largely on the relative disposition of the involved neutral and anionic potential energy surfaces. This has, for example, been instructively described within a classical approach to the temperature dependence of the DEA cross section of the Cl^- formation from CF_3Cl [73]. Fig. 11 shows schematic potential energy curves for the neutral ground state; ABCD, and a strongly repulsive anionic state; $ABCD^-$. The vertical lines indicate the transition to the anionic state at threshold for the vibrational levels $v = 0$–4 and on the right hand site the resulting DEA cross sections are shown schematically for two temperatures for the same vibrational levels. For vibrational levels below the crossing point the threshold energy decreases with increasing quantum number and finally the threshold reaches 0 eV at $v = 5$. In this quasi-diatomic model the dissociation probability is unity when the nuclear distance R is larger than R_C and the dissociation lifetime is fairly well described through Eq. (5). However, the further away from R_C the transition takes place (i.e., at bond lengths shorter than R_C) the shorter is the lifetime of the TNI with regard to autodetachment and the relaxing ion also needs longer time to reach R_C. Hence the dissociation probability decreases. Thus, in general the cross section for DEA increases with increasing vibrational quantum number below the crossing point at R_C but then it decreases gradually again from vibrational levels above the crossing point. The second effect is also due to the reduced overlap of the relevant wave functions when transitions occur further away from R_C. An additional effect comes to play through the inverse energy dependence of the electron attachment cross section at threshold which strongly amplifies the ion signal from transitions close to or at the crossing point (see Eq. (2)). The reflected ion yield curves are shown for two different temperatures in Fig. 11 and the contribution from the individual vibrational levels are indicated by the dotted lines. Fig. 11 visualizes the temperature effect for the case where the ionic curve crosses the neutral one comparatively far to the right of the neutral equilibrium distance R_{Eq}. In this quasi-diatomic description the actual shape of the ion yield curves and the degree to which the 0 eV transition will evolve to a separate peak in the ion yield curves will strongly depend on the relative disposition of the corresponding potentials. However this picture strictly only holds for strongly repulsive direct dissociation processes. When predissociation processes are involved and/or the dissociation coordinate in question is strongly coupled to other vibrational modes of the molecule the temperature dependence of the autodetachment lifetime of the predissociation state can dominate the evolution of the DEA cross section.

Apart from the considerations above, from purely thermochemical considerations one would expect an increase in intensity and a shift to lower energy for endothermic reactions and a decrease in intensity for exothermic reactions with increasing temperature. This is the case for BrCN where the Br^- formation is endothermic by 0.35 eV and the CN^- formation exothermic by 0.13 eV [71]. The Br^- yield increases by an order of magnitude and the maximum in the ion yield curve is shifted from 0.35 eV at room temperature to about 0 eV at 800 K. The exothermic CN^- formation on the other hand decreases by about one order of magnitude in this temperature range [71]. However, this concordance with the thermo-chemical expectations is rather the exception than the rule and already the very similar compound ClCN shows a temperature dependence that can only be explained by the nature of the resonances involved [71]. Both the Cl^- and the CN^- formations are endothermic processes, however only the Cl^- yield increases throughout the temperature range from 300 to 800 K. Furthermore, the Cl^- ion yield maximum is shifted to lower energy as is expected for an endothermic reaction and an apparently new narrow contribution appears at 0 eV. The same observation is made for CN^- up to 600 K, however, above 600 K the CN^- signal drops off rapidly [71]. This may be explained from the fact that the Cl^- formation proceeds directly along a strongly repulsive state (σ^*(X–CN)) as described above, but CN^- is formed through an initial occupation of a low lying π^*(CN) MO and a subsequent vibrational energy transfer into the X–CN coordinate. Hence CN^- is formed through a comparatively slow vibrational predissociation process and the dissociation channel is thus in stronger competition with autodetachment and the reduced autodetachment lifetime prevails at higher temperatures.

A similar effect is observed in 1-bromo-4-chlorobenzene were the Cl^- formation is expected to be almost thermo-neutral and the Br^- formation slightly exothermic [74]. Fig. 12 shows the maxima of the Cl^- and Br^- formation through the low energy peak (0–1 eV) in the temperature range from 300 to 600 K. Using the peak maxima to demonstrate the temperature dependence of the ion yield is justified for 1-bromo-4-chlorobenzene as no distinct 0 eV peak is observed in this case. Both the Cl^- and Br^- ion yields initially increase strongly, go through a maximum at 400 and 460 K for Br^- and Cl^-, respectively, and then rapidly diminish again. Similar to CN^- from ClCN also Cl^- and Br^- from 1,4-C_6H_4ClBr can be understood as predissociation products associated with an initial occupation of a low lying π^* MO which couples to the σ^*(C–X). Thus, at low temperatures the ion yield reflects the formation probability of the ion within the Frank–Condon region and its dissociation

probability. With increasing temperature higher vibrational levels become populated and transitions close to R_C start playing an increasing role. Hence the increased dissociation probability in accordance to Eqs. (4) and (5) and the inverse energy dependence of the initial attachment cross section contribute to the increasing ion yield. With still increasing temperature the population of the relevant vibrational levels goes through a maximum and the density of transitions that take place at larger distance from R_C increases. Thus the time available for autodetachment is extended at the same time as the atodetachment lifetime of the initial TNI is decreased. Hence the ion yield diminishes again. However, in this case it is difficult to distinguish between the role of the shorter autodetachment lifetime of the predissociation state and the extended dissociation lifetime in the quasi-diatomic picture as expressed through Eq. (5). Nevertheless, in this case we have about 30 vibrational degrees of freedom and thus the shortened autodetachment lifetime due to vibrational excitation of the aromatic ring most probably plays the more significant role.

The quasi-diatomic description on the other hand holds well for direct dissociation along a strongly repulsive σ^* state as has been discussed in detail, for example, for CF_3Cl [66,73,75]. Thus one would also expect this to be the case for CH_2ClBr, where only strongly repulsive σ^* states are involved in the DEA process [76]. Indeed, the Br^- yield increases considerably (threefold) when proceeding from room temperature to about 450 K. However, the Cl^- yield decreases to the same extend in this temperature range. Both the Br^- and Cl^- formation are exothermic (by 0.41 and 0.18 eV, respectively) which makes the different behaviour even more puzzling. The increase of the Br^- signal can readily be explained from a strongly repulsive anionic σ^*(C–Br) potential energy curve crossing the neutral potential energy curve at a distance larger than the equilibrium distance (as described above) but the same explanation does not hold for the decrease of the Cl^- yield. However, the assumption that the anionic σ^*(C–Cl) potential energy curve crosses the neutral potential energy curve at shorter distances than the equilibrium distance ($R_C < R_{Eq}$) can explain this observation. In this case the anion is less accessible from vibrationally excited states. Hence heating leads to depopulation of states from which the σ^*(C–Cl) MO can be reached. The same tendency was observed for Br^- generated from $CHCl_2Br$ at 0 eV, whereas the Cl^- yield was independent of the temperature [77].

Finally, for exothermic, direct DEA processes like the Br^- formation from CH_2ClBr the crossing point R_C of the anionic and neutral potential energy curves can be viewed as the activation barrier for the reaction and can be determined from an Arrhenius plot of the temperature dependence. For the Br^- formation from CH_2ClBr the activation energy is found to be 107 meV [76] which should correspond to the energy difference between the crossing point of the two curves at R_C and the ground state of the neutral molecule.

3.1.3. High selectivity in dissociative electron attachment

In DEA it is well established that low energy electrons are highly selective with regard to the bond cleavage and that these selective processes are also often very efficient. Moreover, as this selectivity can often be controlled by simply varying the electron energy within few electron volts DEA may be the optimal tool for the future of chemical control at the molecular level.

In many cases the high bond selectivity in DEA can simply be explained by thermo-chemical constraints, but in other cases the selectivity is exclusively a consequence of the electronic states involved in the initial formation of the TNI. Before discussing the high selectivity of DEA processes it is therefore worthwhile to clarify what is meant by the term *selectivity* in this context.

In general we refer to high selectivity in DEA when only one specific product is formed at specific electron energy. This may be simply due to the thermo-chemical thresholds for the different products formed, in which case we refer to *thermo-chemically controlled selectivity* but it may also be due to only specific dissociation pathways being accessible from the initial electronic states describing the TNI. In that case we refer to *state controlled selectivity*.

If we, for example, consider a diatomic molecule X–Y in which Y is the atom with the higher electron affinity the threshold for the formation of Y^- is lower than for X^-. In DEA to XY one will therefore only observe the formation of Y^- as long as the total energy of the TNI is below the thermo-chemical threshold for the formation of X^-. This might occur over the whole width of a low lying resonance or only the lower energy part of the same, depending on (i) the position of the resonance, (ii) the difference in electron affinity between X and Y and (iii) the bond dissociation energy D(X–Y). Such product selectivity can be observed in direct dissociation along strongly repulsive states but also in predissociation processes. *State controlled selectivity* in DEA on the other hand is observed when only one specific relaxation path is accessible from a given electronic structure of the initially formed TNI. In most cases this leads to the observation of the cleavage of specific bonds at defined molecular sites within a particular energy range. State selectivity may also appear through selective charge retention as is the case for the cyano halides where the charge retention is either on the halogen or the CN group, depending on the initial state. In this section we will discuss few different examples of thermo-chemically controlled selectivity, state selective product formation through bond selectivity as well as through selective charge retention and finally we present an example of state selective formation of a product that requires multiple bond breaking and rearrangements within the molecule. Remarkable bond and site selectivity has also been observed from the nucleobases and has been studied in detail by site specific deuteration and methyl substitution. This will be discussed separately in Section 3.3.1.

The probably most cited examples of selectivity in DEA processes are the halomethanes CF_3Cl [3,46] and CF_3I [3,48,78,79]. Both molecules have purely dissociative $\sigma^*(CF_3–X)$ resonances at low energies. For CF_3I this resonance is located at 0 eV and for CF_3Cl the low energy resonance peaks at 1.4 eV. In both cases the resonance is associated with high kinetic energy release, and in both cases only the heavy halogen ion is observed. This can readily be explained from the energetic thresholds for the individual processes. The I^- formation is exothermic but the CF_3^- formation from CF_3I is endothermic by about 0.7 eV, and while the Cl^- formation from CF_3Cl is close to being thermo-neutral the formation of CF_3^- from this compound requires about 2 eV. Hence, these compounds are excellent examples of thermo-chemically controlled selectivity in direct dissociation processes.

Sulfurhexafluoride (SF_6) is the most extensively studied system with regard to electron attachment (see, for example, refs. [1,80–84] and references therein). At room temperature the molecular ion SF_6^- is observed with exceptionally high cross section at 0 eV ($\approx 10^{-14}$ cm^2 at 0.01 eV) [83]. The ion is understood as a vibrational Feshbach resonance, the lifetime of which is extended with respect to autodetachment and dissociation through intramolecular redistribution of the excess energy. The thermo-chemical threshold for the lowest lying dissociation channel; the SF_5^- formation, is close to 0.12 eV and the thermo-chemical threshold for the next available dissociation channel; the F^- formation is 0.6 eV [2,82]. At room temperature the maximum formation probability of SF_5^- is close to 0.45 eV. At about 300 K and low electron energies the survival probability of the vibrationally excited molecular anion is large and the SF_5^- formation is only observed with relatively low intensities through the higher energy flank of the resonance. With increasing gas temperature the total internal energy of the TNI increases, the maximum formation probability of SF_5^- shifts

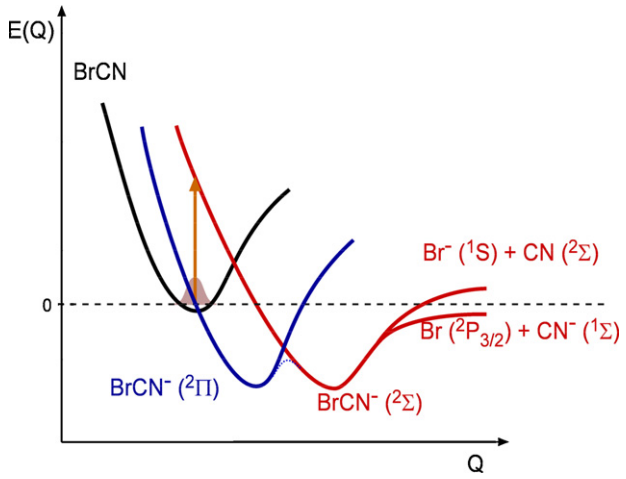

Fig. 13. Schematic potential energy diagram illustrating dissociative electron attachment to BrCN [71]. Transition to the negative ion state $^2\Sigma$ leads to direct dissociation into Br^- and CN. Transition into the $^2\Pi$ surface initially causes vibrational excitation of the CN stretch mode, but CN^- is generated after energy transfer from the C–N coordinate into the Br–CN coordinate (vibrational predissociation).

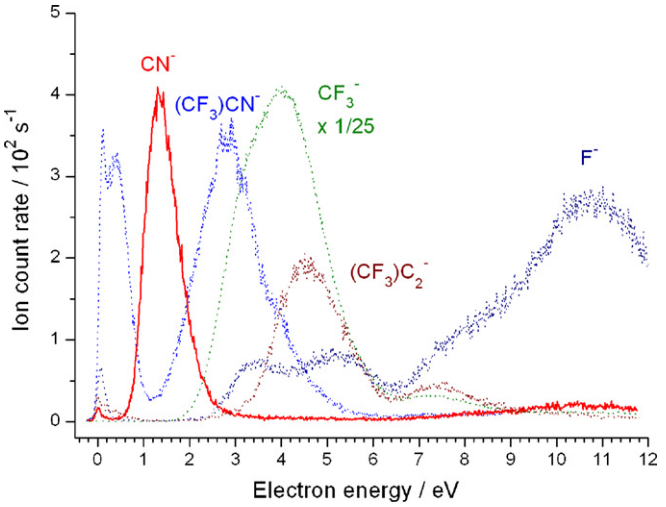

Fig. 14. Ion yields for all fragments observed in DEA to hexafluoroacetoneazine (HFAA) in the energy range from 0 to 12 eV. In the range from 1 to 2 eV only CN^- is formed [85].

to lower energies and the intensity of the SF_5^- signal increases. Finally at sufficient high temperatures (800 K) the SF_5^- signal is shifted to 0 eV and exceeds the SF_6^- signal. For the detailed discussion of this behaviour we refer to reference [82], but essentially we have an endothermic, barrierless dissociation process leading to the cleavage of the SF_5–F bond and due to the lower thermo-chemical threshold only SF_5^- is formed through the low lying resonance peaking at 0 eV. The F^- ion on the other hand is first observed through a purely dissociative resonance centred round 3 eV. From this resonance the SF_5^- ion is also formed with comparable intensities.

A similar situation is observed for the C–Cl bond cleavage in DEA to C_6F_5Cl. The transient negative ion is observed through a narrow peak at 0 eV, the shape and position of which is essentially determined by the lifetime of the vibrationally excited TNI $C_6F_5Cl^{-\#}$. The thermo-chemical thresholds for the formation of the complementary ions are 0.4 eV for Cl^- and between 1.25 and 0.6 eV for $C_6F_5^-$ [3], respectively. The former ion; Cl^-, is formed throughout the whole resonance, peaking at about 0.7 eV. The $C_6F_5^-$ fragment on the other hand is only observed with very low intensities through the very high energy flank of the resonance. At 0.7 eV virtually only Cl^- is formed and the branching ratios where the formation probability is at maximum for both fragments are close to 1:100 in favour of the Cl^- formation [3,61].

A clear and simple example of selectivity which is solely controlled by the initial electronic state of the TNI formed is found in DEA to BrCN described above [71]. Here two different low lying anionic states can be formed; a $^2\Pi$ state located at the CN group and a $^2\Sigma$ state that is formed by a single electron occupation of the strongly repulsive σ^*(Br–CN) MO. Fig. 13 shows a schematic potential energy diagram of the neutral ground state of the molecule and the two negative ion states $^2\Sigma$ and $^2\Pi$. The $^2\Sigma$ state leads to a fast direct dissociation. The shape and energy position in the ion yield curve reflects the whole width of the transition. The vibrational excitation of the CN group in the $^2\Pi$ state must on the other hand find its way into the relevant Br–CN stretch vibration leading to the dissociation of the molecule. In any case, at room temperature the $^2\Pi$ resonance leads explicitly to the formation of CN^- through a narrow contribution at 0 eV, but the $^2\Sigma$ resonance to the formation of Br^- through a broader contribution centred close to 0.3 eV. In this case both channels are thermodynamically accessible and the high selectivity is solely controlled by the initial electronic state of the TNI.

A remarkable selectivity which is clearly controlled by the electronic state of the TNI is observed by the energy selective excision of CN^- from hexafluoroacetoneazine (HFAA); $(CF_3)_2C{=}N{-}N{=}C(CF_3)_2$ [85]. Fig. 14 shows the ion yield for all fragments observed from this compound in the energy range from 0 to 12 eV. The terminal fragments $(CF_3)_2CN^-$, $(CF_3)_2C^-$, CF_3^- and F^- are all observed through higher energy resonances in the range between 2 and 7 eV. In addition the symmetric cleavage leading to the $(CF_3)_2CN^-$ formation is also observed through a double peak with maxima at 0.1 and 0.4 eV, respectively. The CN^- ion is not observed through any of these resonances, but only through one particular TNI state that is centered around 1.35 eV and is not observed on any of the other fragments. Moreover, the CN^- formation is comparable in intensity to the other dissociation reactions and a cross section of about 10^{-22} m^2 is estimated for the process [85]. A closer inspection shows that this very selective excision of CN^- from the center of the molecule requires at least the rupture of two C–C and one N–N bond and the threshold for the reaction as calculated at the MP2/cc-pVTZ level of theory is found to be about 5 eV above the observed threshold [85]. Hence the reaction cannot proceed without new bonds being formed. The most reasonable reaction is the synchronous recombination of the two CF_3 groups to form hexafluoroethane, which would bring the threshold in the vicinity of where it is observed. However, at this point this is still a speculation as is the geometry of the transition state involved and the actual electronic structure of the TNI that explicitly leads to this complex reaction.

3.2. *Formation and evolution of negative ion resonances in a condensed environment*

Electron-induced reactions in condensed phases or at interfaces play a key role in many fields of pure and applied science. This includes surface photochemistry, which is often driven by hot electron transfer to the reactant molecules [86,87], radiation damage of biological material [59,88], reactions stimulated by electrons in scanning tunneling microscopy [89–91], photo-initiated heterogeneous chemistry at surfaces of particles in polar stratospheric clouds [58], and any kind of plasma used in industrial plasma processing [57].

The formation and evolution of negative ion resonances in clusters and on the surface of solids or thin molecular films have been studied on a multiplicity of systems throughout the last decades. In this section we will review some case studies that are prototypical for the evolution of negative ion resonances within molecules in clusters and adsorbed or condensed on surfaces.

Specifically we will discuss (i) suppression and enhancement of DEA channels in ESD of anions and in clusters in comparison to isolated molecules, (ii) negative ion formation through "electron/exciton-complexes" in sub-monolayer adsorbates on multilayer noble gas films and scavenging features in electron attachment to molecular clusters, (iii) narrow low energy ESD features that are absent in DEA to isolated molecules and (iv) low energy electron induced synthesis of new species in thin molecular films and in clusters.

3.2.1. Suppression of DEA channels in ESD

Electron stimulated desorption from various halogenated compounds condensed on surfaces has been studied in Eugens group. These include C_6F_5Cl [3,30], CF_3I [48,79], CHF_2Cl [92–94], $CHFCl_2$ [40], and ClCN and BrCN [95]. In the gas phase under single collision conditions all these compounds show very effective DEA reactions within narrow resonant features below 1 eV. In contrast, desorption of fragment ions from these compounds is observed predominantly from resonant structures located above 4 eV and no desorption is observed below 1 eV. Suppression of ion desorption from low energy resonances is in fact typical when proceeding from DEA to isolated molecules to ESD of anions and may readily be explained by the fast relaxation processes operative in condensates and the energy constraints for ion desorption from surfaces.

Fig. 15 compares the ion yields from DEA to ClCN in the gas phase (Fig. 15a) and ESD of anions from a 7 monolayer (ML) ClCN film condensed on a gold surface (Fig. 15b). In the gas phase the most abundant signals are from the CN^- and Cl^- formation close to 0 eV. Less intense signals are also observed with maxima close to 2 and 6 eV for the CN^- formation and close to 3 and 7 eV for the Cl^- formation, respectively [71]. In the ion desorption spectra the dominating products appear within resonances peaking at 4.3 and 8.8 eV, respectively, and some Cl^- desorption is also observed at about 2.0 eV. The intense low energy resonances on the other hand are completely absent in the ESD spectra (Fig. 15b) [95].

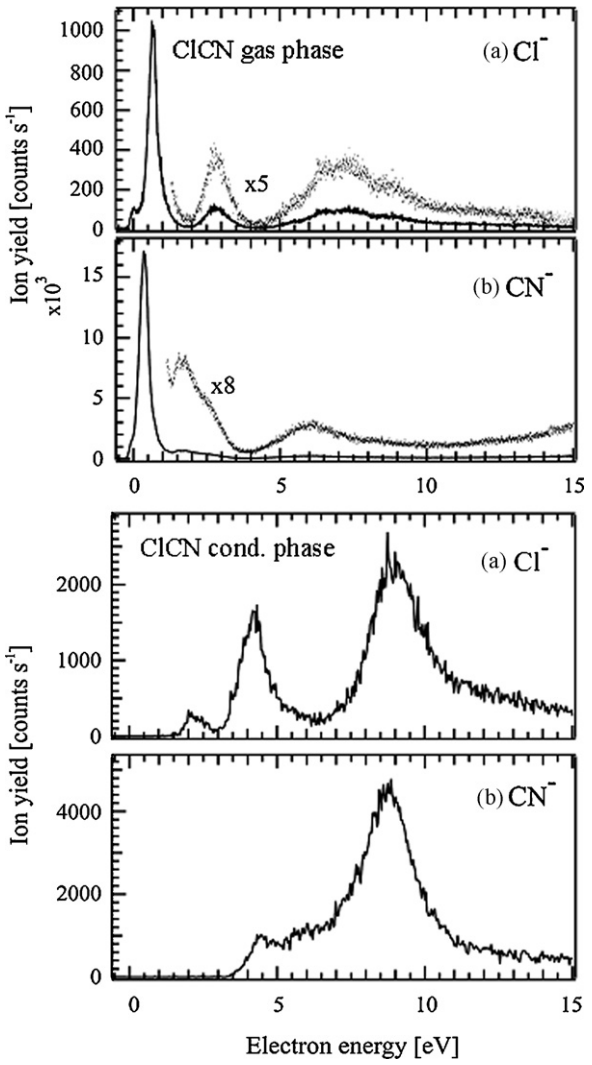

Fig. 15. Comparison between; (a) gas phase DEA yielding Cl^- and CN^- and (b) Cl^- and CN^- desorption from 7 ML ClCN film in the energy range 0–15 eV. Reproduced from Brüning et al. [71] and Tegeder and Illenberger [95] by permission of the American Chemical Society (Copyright 1996) and Elsevier (Copyright 2005), respectively.

If we approximate the decomposition of the TNI at the surface as unimolecular decay and assume the same polarization energy (V_α) for the TNI ($ClCN^{-\#}$) and the fragment ions (Cl^- and CN^-), the energy threshold for desorption (ε_d) can be expressed as

$$\varepsilon_d = \frac{m_i}{m} V_\alpha + \Delta H_0. \quad (14)$$

Here m_i and m represent the mass of the ionic and neutral fragment, respectively. ΔH_0 is the thermodynamic limit for the corresponding gas phase DEA process; 0.58 eV for the Cl^- formation and 0.38 eV for the CN^- formation, respectively [71]. If we estimate V_α to be close to 1 eV [96] we calculate the desorption thresholds to be $\varepsilon_d(Cl^-) \approx 1.8$ eV and $\varepsilon_d(CN^-) \approx 1.1$ eV, respectively. Gas phase ToF experiments [71] indicate a non-thermal formation of both ionic fragments, however, the average kinetic energy release is only 0.25 eV for Cl^- and 0.35 eV for CN^-, respectively. Thus, from the low energy resonance, both fragments are formed with insufficient kinetic energy to overcome the polarization force and can therefore not be observed in the ESD spectra. This does not necessarily imply that electron attachment is no longer operative at the surface. In fact, charging of films of these molecules at low energies (<2 eV) is observed, which indicates that electron attachment is operative, but does not reveal if the attachment process leads to fragmentation or relaxation of the TNI to its thermodynamically stable vibrational ground state.

3.2.2. Stabilization of TNIs and suppression of DEA channels in clusters

In molecular clusters in the gas phase dissociation and autodetachment from low energy resonances may also be efficiently quenched. However, different from ESD where only the ions that can desorb from the surface can be monitored by mass spectrometry, all product ions can be directly monitored in clusters. Hence, in clusters the effect of the reduced escape probability versus the stabilization of the molecular ion can be disentangled. Among the molecules where DEA or autodetachment is efficiently quenched in clusters is the diatomic molecule O_2 [3,31,97–99], the halomethanes CF_3Cl [3,31,47,100] and CF_3I [3,31,48], the haloethanes 1,2-$C_2Cl_2F_4$ [101] and C_2F_5I [102] and the perfluorinated halobenzenes C_6F_5X (X = Cl, Br, I) [3,61].

In electron attachment to the isolated diatomic molecule O_2 only the dissociation product O^- is observed at relatively high energies (6.0 and 7.5 eV, respectively) and no low energy resonances are apparent in the ion yield curves. In clusters on the other hand also

the molecular ion is observed at low energies. The electron affinity of O_2 is well established to be 0.45 eV [103] and autodetachment is only possible from the anion in vibrational states above $v = 3$. Concordantly the stabilisation of O_2^- in clusters is attributed to the fast vibrational energy dissipation within the clusters leading to relaxation of the transient negative ion below $v = 4$ and a partial or total evaporation of the clusters [3,104,105].

In the haloethanes and the halomethanes listed above only DEA is observed in the gas phase under single collision conditions and no molecular ions are detected. This process is observed for CF_3I at 0 eV with high efficiency and considerable kinetic energy release and at 1.4 eV with comparatively less intensity from CF_3Cl. In both cases electron attachment to clusters leads to appreciable formation of the stabilized molecular ion at low energies but the dissociative channels are still operative through the same resonances. This is also true for the haloethanes though the low energy resonance leading to the I^- formation from C_2F_5I is much less efficiently quenched than the corresponding channel leading to the Cl^- formation from 1,2-$C_2F_4Cl_2$. For the halobenzenes on the other hand all dissociation channels through the low lying resonances are quenched. The different behaviour of the aliphatic compounds compared to the aromatic halobenzenes can be attributed to the different nature of the underlying resonances. In the first case the TNI is formed by an occupation of a σ^* C–X repulsive state, leading to a fast dissociation. In the second case the electron initially occupies a low lying π^* MO of the aromatic ring and the excess energy must be transferred into the relevant C–X coordinate. This predissociation is a much slower process which leaves more time for energy dissipation within the cluster before dissociation. Comparable effects are observed for SF_6 and C_6F_6, however, in the latter case no dissociation channels are accessible through the low energy resonance and the molecular ion $C_6F_6^-$ is stabilized with regard to autodetachment [8,38].

In the context of the influence of the initial state of the TNI on the efficiency of the quenching process it would be interesting to study clusters of ClCN and BrCN. Here one would expect quantitative suppression of the predissociation channel leading to the CN^- formation but much less influence on the halogenide formation. Comparable effect should also be expected for propionyl chloride where the Cl^- formation through the π^*(C=O) is likely to be quantitatively quenched but the direct dissociation from the σ^*(C–Cl) state should be much less influenced.

3.2.3. Medium enhanced dissociative electron attachment

A closer inspection of the Cl^- and CN^- spectra from ClCN in Fig. 15 shows that no dissociative attachment products are formed in the gas phase at 4.5 eV and only a weak shoulder is observable around 9 eV in the Cl^- ion yield. This is surprising since the ESD spectra show intense and comparatively sharp desorption resonances at these energies. Due to a variety of different effects such as broadening of transition energies due to inhomogeneous coupling, polarization energy constraints for desorption and energy dissipation within the condensate one would rather expect the opposite effect, i.e., further smearing out of ESD structures compared to those observed in gas phase DEA.

However, coupling of a molecule to an environment can change the character of a resonance in a way that negative ion formation is enhanced (in spite of the many possibilities of energy dissipation). This is particularly the case, when electronically excited resonances are involved. The two prominent desorption features which peak near 4.5 and 8.8 eV in ESD, but are absent in electron attachment to ClCN in the gas phase are most likely core excited resonances. Though no dissociation products are observed in the gas phase at these energies the resonances may still be formed. However, in the gas phase these are open channel resonances

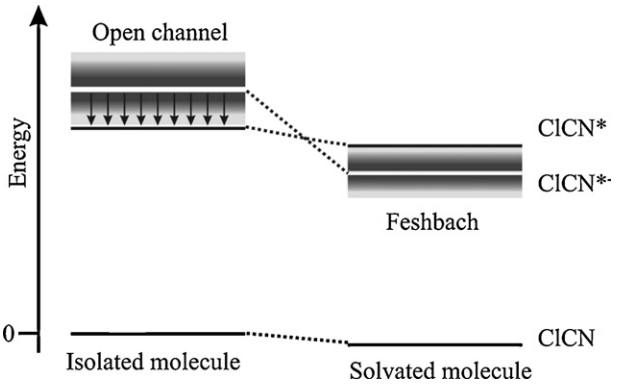

Fig. 16. Schematic representation of the conversion of a short-lived open channel resonance into a Feshbach resonance under solvation. The width of the open-channel resonance is due to Franck–Condon broadening and lifetime broadening. The vertical arrows indicate effective autodetachment (one electron transitions) into the associated electronically excited neutral molecule. The white line indicates the TNI; $ClCN^{*-}$ and the black line indicates the corresponding electronic excited state of the neutral. Reproduced from Tegeder and Illenberger [95] by permission of Elsevier (Copyright 2005).

with autodetachment lifetimes that are typically too short to allow for mass spectrometric observation. In the condensed phase the polarization interaction between the TNI and its environment is considerably stronger than the polarization interaction between the corresponding electronically excited neutral and its environment. If the net polarization interaction is positive this can lead to a stabilization of the TNI relative to the neutral precursor to an extent where the energy of the TNI is lowered below the energy level of the neutral precursor. This is shown in Fig. 16 in a simplified energy-level diagram for the isolated molecule compared to the same molecule in a polarizable environment. In Fig. 16 the total energy of the core excited TNI in the condensed phase is lowered below the corresponding electronically excited neutral molecule and the resonance can therefore only decay to the neutral ground state through a two electron process. Hence a core excited open channel resonance has turned into a closed channel (Feshbach-type) resonance. The lifetime with respect to autodetachment is thus extended which in turn enhances the DEA cross section (see Section 1).

This effect is also observed in clusters, in which case the product ion is either observed after liberation from the cluster or as a part of a larger aggregate of the form M_nX^-. In clusters, however, it can be difficult to unambiguously identify such medium enhanced dissociation, as self-scavenging processes can produce comparable features. This is however only true if DEA is still operative at low energy. In the case of the pentafluoro halobenzenes C_6F_5X the conversion of a core excited open channel resonance to a closed channel resonance is observed in all four compounds. In these cases the halogen ion X^- is formed in aggregates at about 6.5 eV whereas electron attachment to isolated C_6F_5X molecules does not lead to any appreciable ion formation at this energy. In C_6F_5X the low energy dissociation channels are close to being quantitatively quenched [3,61]. Hence the new feature at 6.5 eV cannot result from self-scavenging within the cluster. The conversion of core excited open channel resonances to closed channel (Feshbach) resonances is also observed in clusters and condensates of CF_3I [3,48,79]. In this particular case I^- is still produced at low energy in clusters which makes it difficult to exclude self-scavenging from the new I^- feature appearing close to 6 eV in clusters. However, CF_3^- which is not produced below 1 eV (neither in isolated molecules nor in clusters) is also produced in clusters at 6 eV with appreciable intensities.

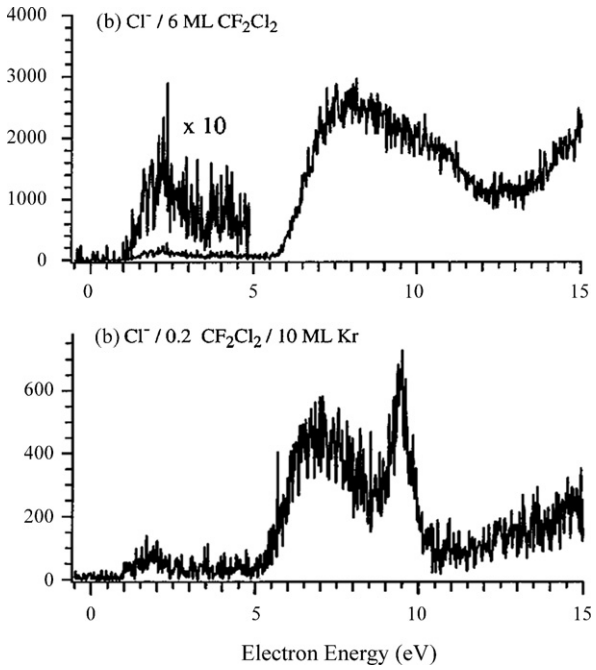

Fig. 17. Desorption of Cl^- from a 6 ML CF_2Cl_2 film condensed directly on a gold surface (upper panel) and from a 0.2 ML condensed on a 10 mL Kr film. Reproduced from Langer et al. [108] by permission of the American Institute of Physics (Copyright 2000).

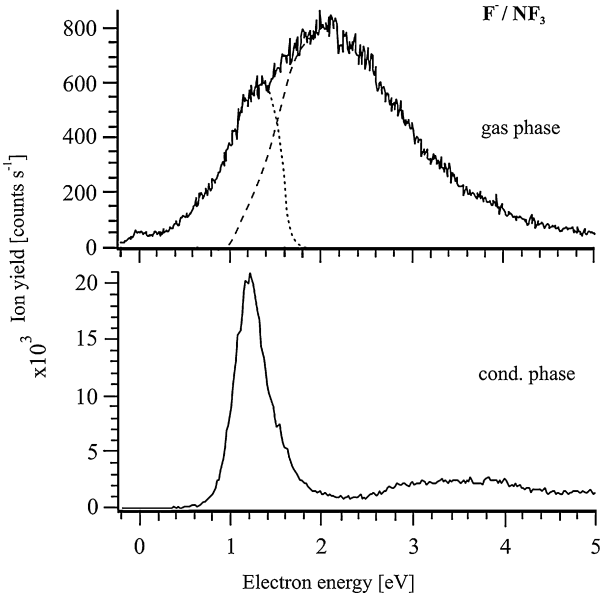

Fig. 18. Comparison between gas phase F^- yield from DEA to NF_3 (upper panel) and the desorption of F^- from a 5 ML NF_3 film (lower panel). Both spectra are recorded from 0 to 5 eV. The dashed line in the gas phase spectrum indicates the overlapping two resonances (see text). Reproduced from Tegeder and Illenberger [109] by permission of RSC Publishing (Copyright 1999).

3.2.4. Negative ion formation through noble gas "electron/exciton-complexes"

In addition to the medium enhanced dissociative electron attachment features described above ion desorption may also be enhanced when molecules are adsorbed in sub-monolayer amounts on Xe or Kr substrates. These features are typically much narrower than the usual ESD features and appear always at the same energy for a given noble gas substrate. Such resonances have, for instance, been observed for H^- and D^- desorption from D_2O, H_2O, C_2D_6, and C_6D_6 [106,107], Cl^- from $CFCl_3$ [43], F^- from SF_6 [38,42] and Cl^- from CF_2Cl_2 [108]. Fig. 17 displays exemplary Cl^- desorption from 6 ML CF_2Cl_2 directly condensed on the gold surface compared to the Cl^- desorption from 0.5 ML CF_2Cl_2 adsorbed on 10 ML Kr. In addition to the desorption features normally observed from multilayers of CF_2Cl_2, strong resonant enhancements in the ESD yield of Cl^- appears at 9.82 eV [108]. In the case of Xe this narrow feature appears at 7.95 eV. The corresponding negative ion states are well known for the isolated rare gas atoms (e.g., Kr^{*-} ($4p^25s^2$) at 9.52 eV). In both cases these resonances are located approximately 0.5 eV below the lowest excited state of the neutral atom. This enhancement is therefore explained by the initial formation of an "electron/exciton complex" in the rare gas film, viz. an extra electron bound to an exciton in the noble gas solid (the analogue to an anionic Feshbach resonance in single atoms). The electron/exciton complex transfers its electron and energy in the case of CF_2Cl_2 to form a dissociative state of $CF_2Cl_2^{*-}$ which relaxes to form Cl^-.

3.2.5. Auto- and self-scavenging features from clusters

Negative ion formation mediated through noble gas "electron/exciton-complexes" have also been observed in mixed O_2/Ne and O_2/Ar clusters [99]. However, within clusters, processes where the incoming electron looses its energy in an inelastic scattering event and is subsequently captured by another molecule are more commonly observed. A prerequisite for this process to take place is that the cluster is at least partly composed of molecules that have comparatively high cross section for electron attachment close to 0 eV. Self-scavenging processes in CF_3I and the pentafluoro halobenzenes C_6F_5X (X = Cl, Br, I) as well as auto-scavenging processes in mixed O_2/N_2 and SF_6/N_2 clusters have been discussed in detail in the reviews [3,31] and references therein. We therefore refrain from detailed discussion here. However, a fairly detailed discussion of auto-scavenging within C_6F_5Cl/N_2 clusters in comparison with SF_6/N_2 may be found in the supplementary material to this review.

3.2.6. Narrow resonances in low energy desorption

As mentioned above, suppression of low energy resonances is in fact typical when proceeding from DEA to isolated molecules to ESD of anions from adsorbed or condensed molecules. An exception is NF_3 where electron attachment to multilayer NF_3 films leads to a remarkably intense desorption of F^- ions at low electron energies [109]. Fig. 18 compares the F^- yield from DEA to NF_3 in the gas phase (upper panel) to ESD of F^- from a 5 ML NF_3 film condensed on a gold substrate (lower panel). The dominant low energy (0–4 eV) desorption features show two energetically separated comparatively narrow resonances. The first has a maximum at 1.2 eV and the second close to 3.5 eV. The gas phase F^- spectrum on the other hand exhibits only one broad and unresolved resonance in this energy range [110]. This is a rather surprising observation as from most of the previous studies the opposite effect was observed, i.e., quenching of low energy DEA fragments and a smearing out of structures when going from DEA to isolated gas phase molecules to ESD from condensates.

A closer look reveals that this behaviour can be explained by the particular energy constrains for ion desorption in relation to the energetics of the DEA reaction leading to the F^- formation/desorption. The kinetic energy analysis of F^- ions from gas phase NF_3 [22] showed that in the energy range up to ≈2 eV F^- ions with appreciable kinetic energy are generated. Above that energy, on the other hand, a low kinetic energy component appears and becomes more dominant towards higher electron energy. This was

interpreted by the existence of two different, energetically overlapping TNI states. One being related to the electronic ground state of the anion and the other to an electronically excited state, i.e., a core excited resonance. The precursor ion associated with the electronic ground state decomposes via direct dissociation for which the associated kinetic energy distribution was shown to be quasi-discrete and when the primary electron energy is increased from 0.2 to 2 eV the mean kinetic energy of the F^- ions from this resonance increased from 0.7 to 1.5 eV. In contrast, the electronically excited precursor decomposes into F^- with a quasi-thermal energy (the mean kinetic energy of F^- is below 0.3 eV), indicating a less direct decomposition mechanism.

This explains the difference between the gas phase DEA spectra and the desorption yield in the ESD experiments. The low energy precursor state ejects F^- ions with appreciable kinetic energy hence they contribute significantly to the desorption yield. The dissociation of the core excited TNI on the other hand, yields a quasi-thermal kinetic energy distribution and only a small fraction within the high energy tale of the translational energy distribution has sufficient energy to overcome the polarization barrier and thus leave the surface. This results in a comparatively low desorption yield from the second resonance but also an appreciable shift of its maximum in the ESD yield with respect to that of the gas phase analogue by more than 1 eV.

3.2.7. Electron induced synthesis within molecules condensed on surfaces

So far we have only considered unimolecular decay reactions of TNIs formed in clusters or within molecules adsorbed or condensed on surfaces. However, low energy electrons can also induce reactions that result in the generation of new neutral molecules [111–114]. These must be monitored by different means than ESD of ions. One approach is to probe such reactions by surface vibrational spectroscopy [44], but also changes in the desorption behavior resulting from the formation of new products at the surface [115–118] can be used to monitor reactions. One example of reactions induced in molecular films by low energy electrons is the transformation of NF_3 to NF_2 and N_2F_2 through exposure to low energy electrons. The (relative) degradation cross section of NF_3 is extracted by IRAS by monitoring the intensity loss of the asymmetric stretch vibration of NF_3 as a function of electron dose at variable electron energies. Fig. 19 displays the electron energy dependence of the (relative) degradation cross section of a 10 ML NF_3 film (left panel) compared to the F^- yield from DEA to isolated NF_3 molecules in the gas phase [110] and to ESD of F^- from a multilayer NF_3 film condensed on the metal surface [109] (right panel). The cross section for the intensity loss peaks at low energy near 4 eV and increases again at energies above 6 eV. This behavior can directly be related to the electron capture properties of the target molecule as can be seen by comparing the both panels in Fig. 19. From the energy dependence we conclude that the degradation cross section at low electron energies is directly related to resonant electron capture as the initial process. This is in fact the only process which can initiate chemical changes in that energy domain. At higher energies, however, inelastic scattering and subsequent capture of the slowed down electron (self-scavenging) may play a significant role, but also non-resonant processes such as dipolar dissociation and ionization may contribute. An extended IR analysis of the NF_3 film after electron irradiation showed that irradiation at 1.5 eV creates NF_2 radicals and N_2F_4 molecules. The latter may be formed by the exothermic association of two adjacent NF_2 radicals. In contrast, exposure to 8 eV electrons gives evidence for NF and NF_2 but not N_2F_4 formation. This may indicate that N_2F_4 which is possibly formed at 8 eV is degraded by subsequent electron collisions and that N_2F_4 degradation is not (or less) operative at low electron energies.

Another example of electron induced reactions at surfaces is the transformation of 1,2-$C_2F_4Cl_2$ molecules into Cl_2 and possibly perfluorinated polymers after irradiation with 9 eV electrons [32,115,116]. In fact Cl_2^- resulting from low energy electron induced unimolecular decay is observed directly from isolated molecules and molecular clusters of 1,2-$C_2F_4Cl_2$ [101], and such formation of dihalogen ions is also observed from other halogenated compounds [46].

However, also considerably more complex reactions have been observed in clusters. One of these is the nucleophilic substitution reaction in which the nucleophile is generated through a DEA process in a binary cluster. The nucleophile then attacks the target molecule and the leaving group or the ion molecule complex is detected. These reactions have been studied on the systems $F^- + CH_3X$ where the leaving group is either Cl^-, Br^- or I^- and the nucleophile; F^- is generated either by electron attachment to C_2F_6 [119,120] or NF_3 [121]. The nucleophilic substitution reaction could also be observed in the system $Cl^- + CH_3Br$, in which Cl^- was generated at 0 eV from CCl_4 [120]. Fig. 20 shows the ion yield curves recorded from homogeneous CH_3Cl, CH_3Br and CH_3I clusters gener-

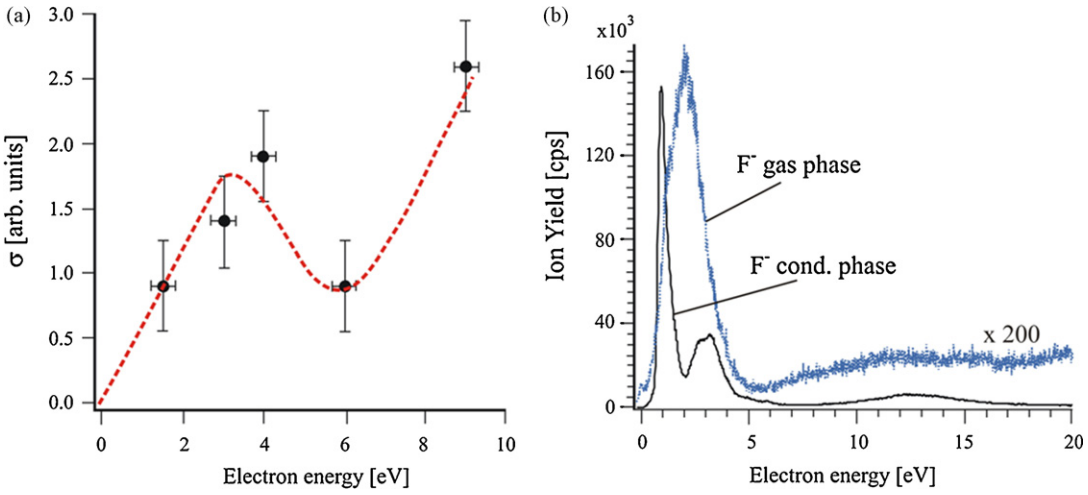

Fig. 19. The left panel shows the relative degradation cross section of the asymmetric stretch vibration of NF_3 recorded with IRAS from a 10 ML film as a function of the electron energy at given electron dose. The right panel compares the F^- formation from isolated NF_3 molecules in the gas phase and from the NF_3 film at a thickness of 10 ML used for the IRAS studies. Reproduced from Tegeder and Illenberger [44] by permission of Elsevier (Copyright 1999).

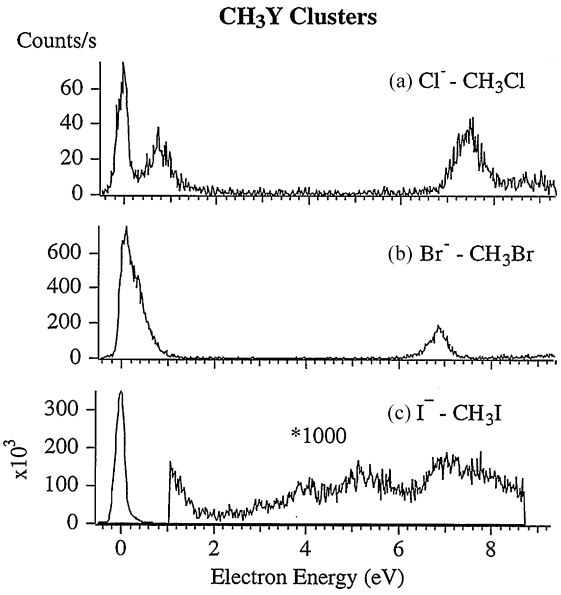

Fig. 20. Ion yield curves recorded from CH_3Cl, CH_3Br and CH_3I clusters generated by a 1:10 CH_3X:Ar expansion. No Br^-, Cl^- or I^- ion yield is observed in the energy range between 2 and 6 eV and only weak contributions of I^- in the spectrum of CH_3I. Reproduced from Lehmann and Illenberger [120] by permission of Elsevier (Copyright 1999).

ated by an 1/10 argon expansion [120]. It is clear from these spectra that virtually no Cl^-, Br^- or I^- is produced from CH_3Cl, CH_3Br and CH_3I in the energy range from 2-6 eV. Fig. 21 shows the F^- yield from homogeneous C_2F_6 clusters and the X-yield from binary C_2F_6/CH_3X (X = Cl, Br, I) clusters generated by co-expansion of CH_3X mixed with argon [120]. In the binary clusters the same resonance profile as appears for the F^- formation from C_2F_6 also appears with considerable intensity in the ion yield curves for X^- from CH_3X. This is explained by a nucleophilic substitution reaction in which F^- generated in the binary cluster through DEA to C_2F_6 attacks a CH_3X molecule within the same cluster, i.e.;

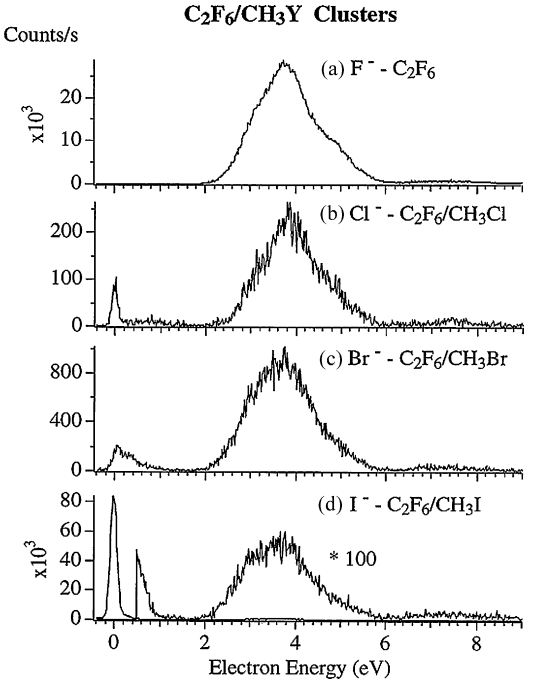

Fig. 21. Ion yields from binary C_2F_6/CH_3X (X = Cl, Br, I) clusters generated by co-expansion of CH_3X and C_2F_6 mixed with argon. In the binary clusters the resonance profile for the F^- formation from C_2F_6 appears in all compounds with considerable intensity on the X^- signal. Reproduced from Lehmann and Illenberger [120] by permission of Elsevier (Copyright 1999).

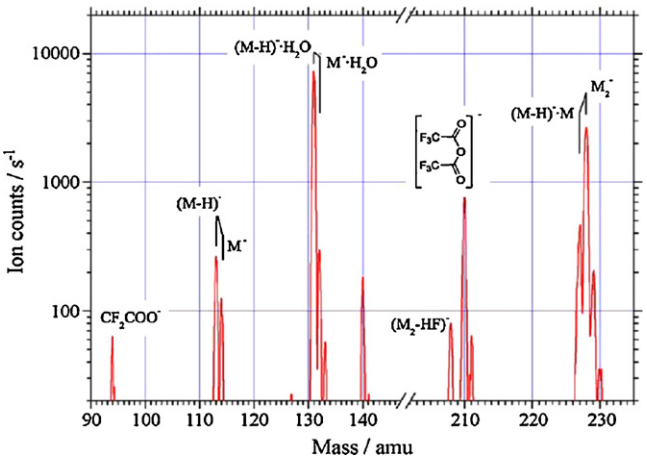

Fig. 22. Negative ion mass spectrum from an expansion of CF_3COOH seeded in argon (1/30) recorded at an electron energy of 0.3 eV. The dominant peak at 131 amu is assigned to the complex $H_2O{\cdot}CF_3COO^-$ arising from electron capture by a dimer and the peak at 210 amu is assigned to the acid anhydride anion. Reproduced from Langer et al. [122] by permission of Elsevier (Copyright 2006).

$$C_2F_6 + e^- (\varepsilon = 2\text{–}6\,\text{eV}) \rightarrow F^- + C_2F_5 \quad (15)$$

$$F^- + CH_3\text{–}X \rightarrow [F\text{–}CH_3\text{–}X]^- \rightarrow F\text{–}CH_3 + X^- \quad (16)$$

For binary NF_3/CH_3Cl and CCl_4/CH_3Br clusters virtually the same effect is observed, except that in the latter cases the S_N2 reaction takes place close to 0 eV electron energies.

Recently also the dehydration reaction and the anhydride formation in organic acids was shown to occur in clusters of trifluoroacetic acid (TFAA) upon low energy electron irradiation [122]. The negative ion spectrum of CF_3COOH clusters recorded at 0.3 eV is shown in Fig. 22. The spectrum is dominated by the regression of M_n^- and $M_{n-1}(M\text{–}H)^-$ (not shown here), but three additional prominent peaks appear in the spectra below 250 amu. These are at 94, 131 and 210 amu, respectively, and are attributed to CF_2COO^-, $H_2O{\cdot}CF_3COO^-$ and to the anhydride; $(CF_3CO)_2O^-$. The latter two ions are both the result of a bimolecular reaction within the cluster as was confirmed for the complex ion; $H_2O{\cdot}CF_3COO^{*-}$, by electron attachment to the deuterated TFAA. Furthermore, the generation of these products show extraordinary size selectivity, and as no solvated products are observed they are most likely exclusively produced from the dimer.

3.3. Low-energy electron interaction with biomolecules

It has long been known that low energy (<20 eV) electrons are abundant along the ionization track of high energy radiation, however, only recently it was shown that such low energy electrons can in fact induce single and double strand breaks in plasmid DNA [88]. Moreover, the characteristic profile of the yield curves of DNA strand breaks [88,123] suggest that dissociative electron attachment plays a pivotal role in these processes. These finding triggered a substantial research effort that aims towards a detailed understanding of the underlying mechanisms [59].

Eugen and co-workers have contributed significantly to this research field and were in fact the first who could show that the gas phase DNA nucleobases thymine and cytosine are subject to dissociative electron attachment [124]. In the meantime electron-induced reactions have been studied in the gas and

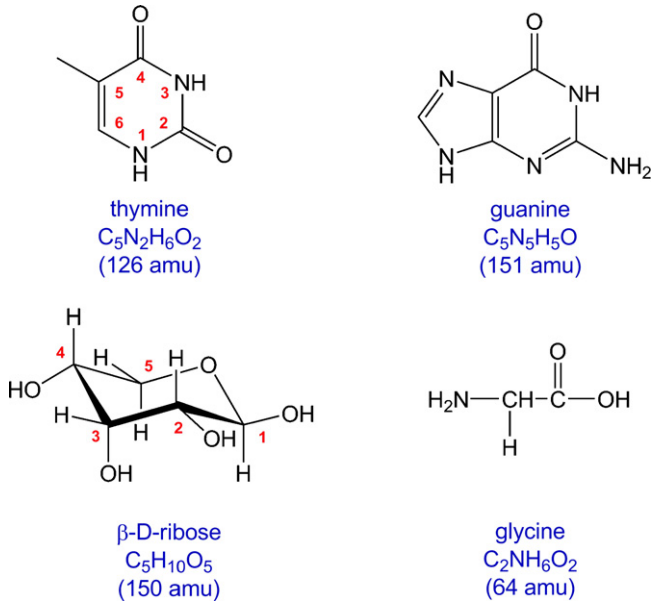

Fig. 23. Molecular structures of the nucleobases thymine and guanine, the monosaccharide D-ribose and the amino acid glycine. For thymine and D-ribose the atom labeling is shown.

condensed phase with several classes of biomolecules including nucleobases [125–133], the monosaccharides ribose [134,135] and deoxyribose [136], phosphodiesters [137], and aminoacids [138–147]. Very recently also electron attachment to intact thymidine was successfully demonstrated in the gas phase [51,52]. In addition experiments on the interaction of low energy electrons with self-assembled monolayers of oligonucleotides approach the investigation of biomolecular systems from another level of complexity [148,149].

In this section we try to give an overview of Eugens work on different aspects concerning electron interaction with biomolecules such as nucleobases, sugars and amino acids. This includes (i) site and energy selective reactions in nucleobases and sugars, (ii) complex rearrangement reactions at very low energies, (iii) molecular mechanisms of DNA radiation damage, and (iv) new experimental techniques to study electron induced reactions in larger biomolecules.

3.3.1. Site selective fragmentation reactions

The most dominant fragmentation reaction observed in DEA to the nucleobases (NB) is the abstraction of a hydrogen atom from the TNI at energies between 0.5 and 3 eV [132]:

$$e^-(< 3\,eV) + NB \rightarrow NB^{-\#} \rightarrow [NB\text{–}H]^- + H \quad (17)$$

In the pyrimidine nucleobase thymine (T) the loss of H can be due to a C–H or N–H bond cleavage (Fig. 23). In deuterium labeled thymine (T_D) [125], where only the C sites of the molecule are deuterated only the fragment ion $[T_D\text{–}H]^-$ is observed and no ion signal from $[T_D\text{–}D]^-$ was detected. Moreover, the fragment ion $[T_D\text{–}H]^-$ exhibited identical ion yield curves as the non-deuterated thymine. This shows clearly that the TNI; $T^{-\#}$, formed at low energies decays exclusively by N–H bond cleavage while no C–H bond cleavage is operative at these energies. However, in the free pyrimidine bases the N–H bond rupture can proceed either from the N1 or the N3 site. Fig. 24 compares the $[T\text{–}H]^-$ ion yield from thymine that is methylated at N1 (m1T) with the yield from non-methylated thymine (dotted line) and the $[U\text{–}H]^-$ yield from uracil methylated at N3 (m3U) with the non-methylated uracil (dotted line) [130]. It is evident from Fig. 24 that the low energy signal at 1 eV

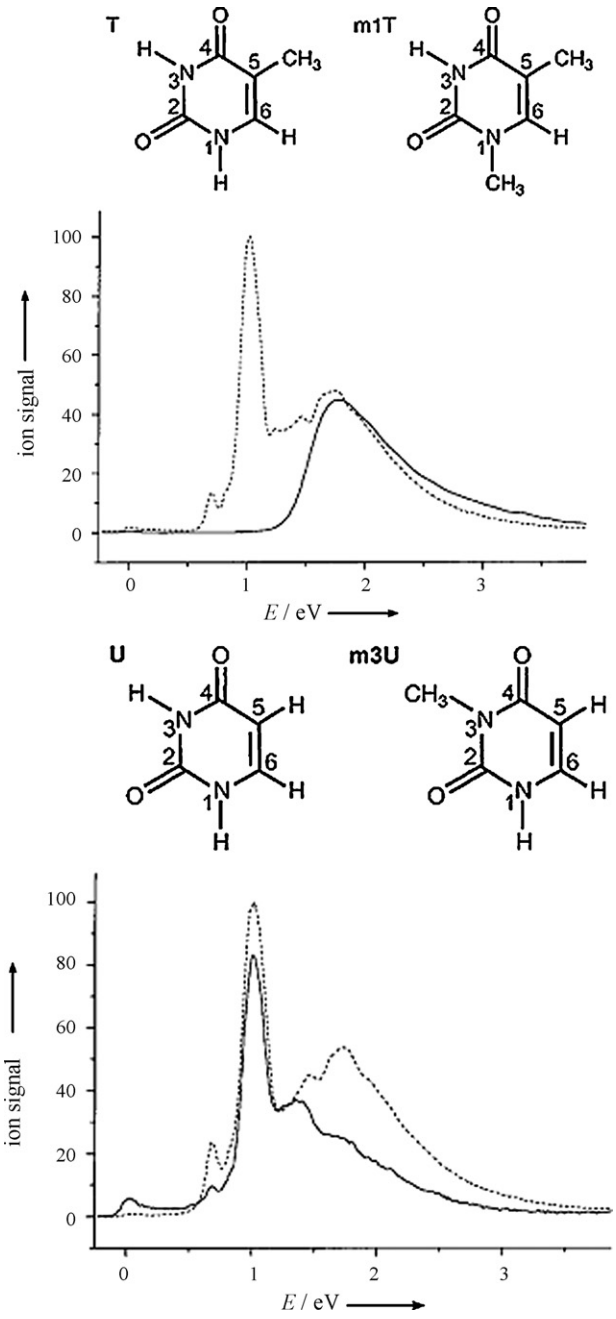

Fig. 24. Anion yield of the $[M\text{–}H]^-$ fragment anion generated by electron attachment to thymine methylated at the N1 position (top), and uracil methylated at the N3 position (bottom). The dotted curve shows the non-methylated thymine and uracil, respectively. It is clear from the spectra that H loss up on DEA occurs from the N1 site at electron energies around 1 eV, whereas the H loss occurs from the N3 site at an incident energy of 1.8 eV. Reproduced from Ptasinska et al. [130] by permission of Wiley-VCH Verlag (Copyright 2005).

vanishes when N1 is blocked and the contribution around 1.8 eV diminishes considerable when N3 is blocked. Hence the low energy signal peaking at 1 eV is due to H loss from N1, whereas the second signal peaking at 1.8 eV arises from N3–H bond breaking. Consequently the observed hydrogen abstraction reaction is not only bond selective, but also site selective at particular electron energy. This can partly be rationalised by energetic considerations [130], but also by the specific shape of the involved molecular orbitals [131].

At higher electron energies (>5 eV) the cleavage of the hydrogen bond results exclusively in the formation of the hydrogen ion [126]:

$$e^-(> 5\,eV) + T \rightarrow T^{-\#} \rightarrow [T\text{–}H]^\bullet + H^- \quad (18)$$

The H^- signal is composed of at least four contributions peaking at 5.5, 6.8 and 8.3 eV, and a distinct shoulder at 9.3 eV [126]. For thymine, isotope labeling revealed that the two lower energy resonances at 5.5 and 6.8 eV, respectively, arise from an N–H bond cleavage, whereas H^- at 8.3 and 9.3 eV is generated from the C–H sites of thymine [126]. Furthermore, methylation of thymine and uracil at N1 and N3, respectively, shows unambiguously that the most pronounced resonance in this region; the 5.5 eV resonance, is exclusively due to N3–H bond cleavage [130].

Site selective generation of anion fragments was also observed in the monosaccharide D-ribose [135]. D-Ribose in the gas phase is a six-membered ring with four C–C bonds and two C–O bonds (Fig. 23). At very low energies close to 0 eV a transient negative ion is generated that decomposes into various fragments associated with production of neutral water and formaldehyde molecules (CH_2O). A characteristic reaction that is accompanied by a decomposition of the ring system is the formation of an anionic fragment at 72 amu:

$$e^-(\approx 0\,eV) + C_5H_{10}O_5 \rightarrow C_5H_{10}O_5{}^{-\#} \rightarrow C_3H_4O_2{}^- + 2CH_2O + H_2O \quad (19)$$

Also the formation of $C_3H_4O_2{}^-$ at 71 amu is observed with comparable intensities. Fig. 25 shows the ion yield for the masses 71 and 72 amu from 5-^{13}C-D-ribose (left) and 1-^{13}C-D-ribose (right) [135]. The 5-^{13}C-D-ribose shows no mass shift for neither of the fragments but with the 1-^{13}C-D-ribose the signals are shifted by one mass unit. Hence this reaction exclusively proceeds by the loss of C5. The same observation is made for the masses 101 and 102 amu associated with the formation of $C_4H_5O_3{}^-$ and $C_4H_6O_3{}^-$, respectively.

3.3.2. Complex rearrangement reactions

Apart from single bond cleavages as described above, electron attachment to nucleobases can also lead to a decomposition of the aromatic ring system. These resonant reactions which typically take place between 3 and 10 eV [124,129] result in the formation of CN^- and OCN^- among other fragments. These are both well-known pseudohalogens with high electron affinities (3.82 and 3.61 eV for CN and OCN, respectively). Fig. 26 shows the ion yield curves for guanine in the range from 0 to 15 eV. In guanine, opposite to the other bases fragmentation of the ring system dominates and $[G\text{–}H]^-$ is only observed with low intensities [129]. The dominating fragments are OCN^- and CN^- which are already formed with appreciable intensities below 3 eV. In the case of CN^- this reaction requires the cleavage of at least three bonds within the aromatic ring system (Fig. 23). It is therefore clear, that this decomposition of the TNI involves complex multiple fragmentation reactions and may involve new bond formations, however, it should be noted that in case of guanine a partial decomposition may take place in the thermal evaporation process. This is however less likely for the pyrimidine bases where the decomposition of the ring and the formation of the pseudo halogenide ions is also observed with comparatively high intensity [124].

The pseudo-halogenide CN^- was also observed in electron attachment to several amino acids. Among these, the aliphatic amino acid glycine has been studied most extensively with regard to energy dependence of the CN^- formation [139,147,150]. In glycine CN^- is generated from a shape resonance located close to 1.2 eV and a core excited resonance located at 6 eV and close to 10 eV. For

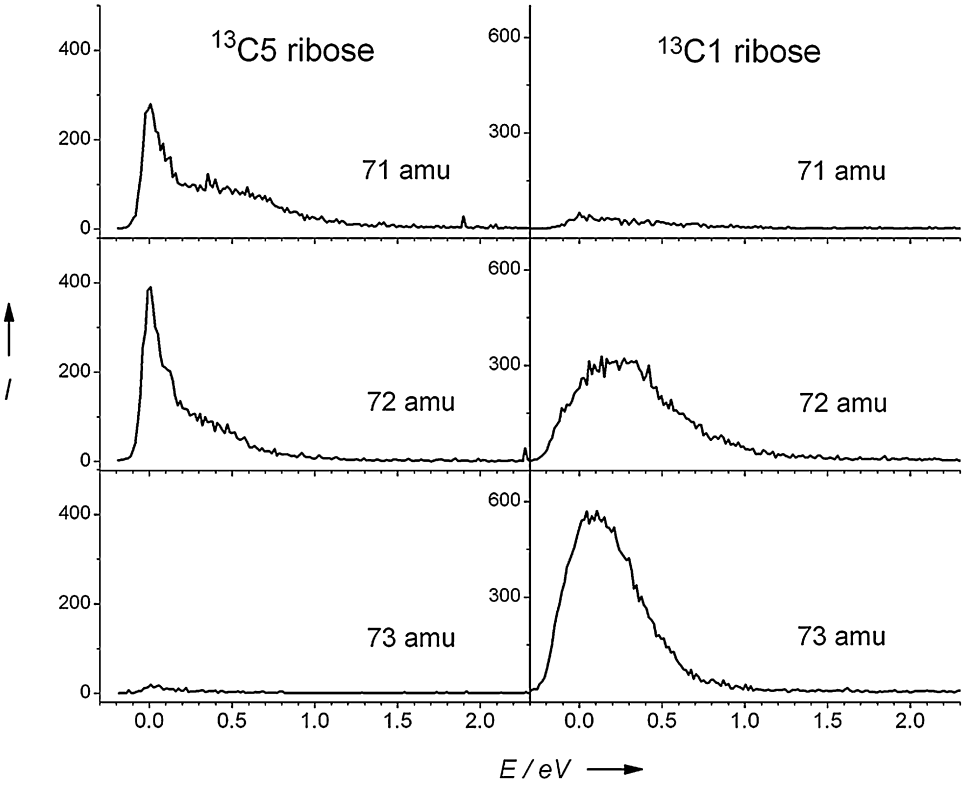

Fig. 25. Anion yields of the 71 and 72 amu fragments generated from 5-^{13}C-D-ribose (left) and the 1-^{13}C-D-ribose (right). In the 5-^{13}C-D-ribose the signals are not shifted, whereas both signals shifted to 72 and 73 amu, respectively, in 1-^{13}C-D-ribose. This shows that the neutral unit(s) is exclusively formed by excision of the C5 carbon. Reproduced from Bald et al. [135] by permission of Wiley-VCH Verlag (Copyright 2006).

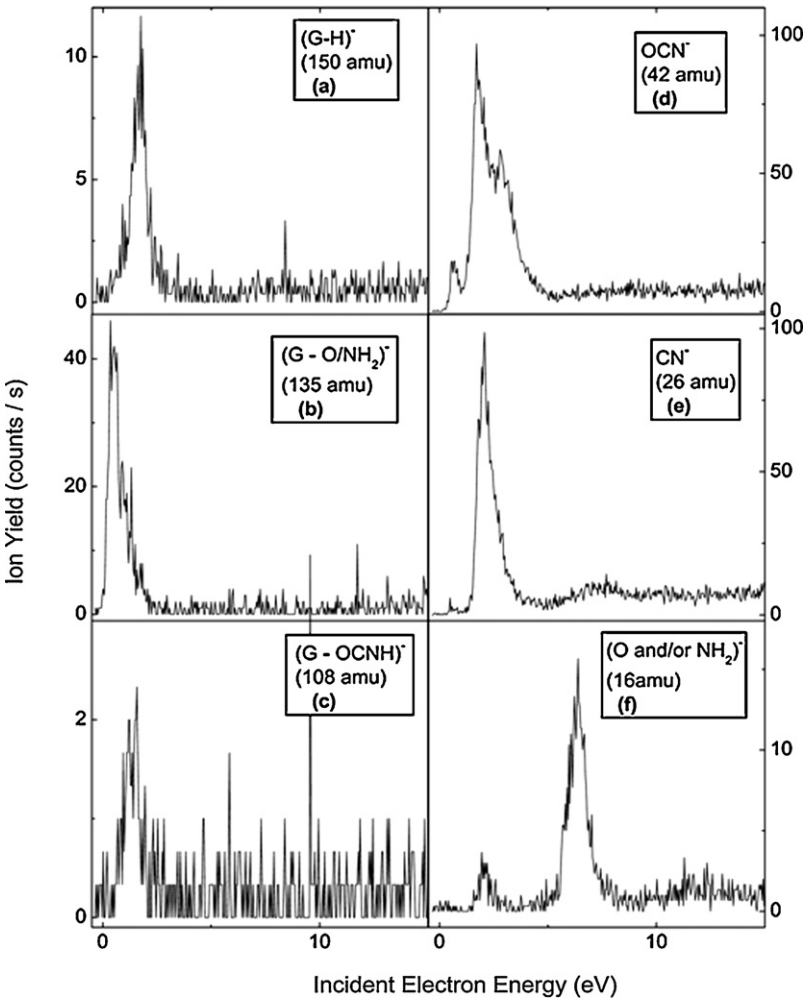

Fig. 26. Fragment anions formed by dissociative electron attachment to guanine in the electron energy range from 0 to 15 eV. For the production of CN^- (middle right) at least three bonds must be broken. Reproduced from Abdoul-Carime et al. [129] by permission of Springer–Verlag (Copyright 2005).

this reaction five bonds have to be broken and if no new bonds are formed the threshold for the reaction is above 10 eV. Thus new bonds must be formed for the reaction to be thermodynamically possible. According to the reaction

$$e^-(1.2\,eV) + H_2NCH_2COOH \rightarrow CN^- + CO_2 + 2H_2 + H \quad (20)$$

the thermodynamic threshold would be around 2.6 eV [139]. However, in context of the CN^- formation from valine also the following alternative reaction scheme has been suggested;

$$e^-(1.2\,eV) + H_2NCH_2COOH \rightarrow CN^- + COOH + 2H_2, \quad (21)$$

Here the energetic threshold would be close to 0 eV and the CN^- formation would be readily accessible through the low lying resonance [146].

Substantial rearrangement is also required for the generation of all fragment ions observed in DEA to D-ribose [135] (see previous section). Nevertheless, most of these reactions are observed close to 0 eV. The simplest reaction observed in D-ribose is the abstraction of a water molecule:

$$e^-(\approx 0\,eV) + C_5H_{10}O_5 \rightarrow C_5H_{10}O_5{}^{-\#} \rightarrow C_5H_8O_4{}^- + H_2O \quad (22)$$

For this reaction at least two bonds must be broken, and even if the electron affinity of the precursor to the remaining ion $C_5H_8O_4^-$ is relatively high, new bonds must be formed for this reaction to proceed close to 0 eV. However, though new bond formation may account for the thermodynamic thresholds for these complex fragmentation reactions, it is still remarkable that they proceed at such low energies as this requires the corresponding transition states to be formed with a very low activation barrier or that the processes are basically barrierless.

3.3.3. The molecular mechanisms of electron-induced DNA strand breaks

For a complete description of the role of low energy electrons for DNA damage by ionizing radiation the reader is referred to more detailed reviews on the subject [32,59]. Here we will only discuss some aspects of electron-induced DNA strand breaks that are revealed by DEA studies to gas phase DNA components.

To date, contradictory models are proposed on how low energy electrons damage DNA. The yields of DNA strand breaks [88,123] show distinct maxima at 1 eV, between 2 and 3 eV and around 10 eV. Experiments on single building blocks of DNA indicate that at these different energies different electron attachment and fragmentation mechanisms contribute to the strand break yield.

As was discussed above, all nucleobases (NB) undergo dissociative electron attachment within two resonant features at 0–4 eV and at higher energies between 6 and 12 eV. The high energy resonances lead to the formation of H^-, but also to degradation of the ring structure. From the low energy contributions an abstraction of the neutral H atom occurs exclusively from the N-sites thereby

forming the closed shell $[NB–H]^-$ anion. It is thus not obvious that electron capture by the nucleobases leads to strand breaks within the DNA chain. However, if the extra electron initially captured by the nucleobase causes charge transfer to the backbone it may indirectly induce a strand break by bond cleavage, for instance, between the sugar and phosphate moiety. This transfer mechanism was however investigated by theory [151], and was predicted to occur with low reaction rates compared to the autodetachment lifetime. Furthermore DEA studies on the nucleoside thymidine [51,52,152,153] indicate that localization of the extra electron on the nucleobase does not lead to dissociation reactions within the sugar moiety. In other words, a charge transfer between nucleobase and sugar moiety in thymidine does not take place. The situation may, however change if a phosphate group is present. Furthermore, besides the direct damage caused by DEA, damage can also arise from secondary reactions with reactive neutral radicals (e.g., the H radical) generated by DEA to the bases. This may lead to clustered damage that is difficult to repair by enzymes and is thus much more severe than a single strand break. However electron attachment to DNA via the nucleobases is not the only mechanism that can lead to strand breaks. As a strand break finally occurs within the DNA backbone it is reasonable to consider a direct electron attachment by the backbone subunits. Different model systems for the sugar and the phosphate moiety have been investigated with respect to DEA. The sugar unit was mimicked by isolated monosaccharides [135,154] and sugar esters [155], and for the phosphate group phosphate esters [137] were used as surrogates. At very low energies close to 0 eV electrons are captured by both the sugar and the phosphate unit and in both cases the low energy electrons induce dissociation reactions that involve considerable rearrangement (see previous section). The dissociation of the sugar is characterized by a loss of different numbers of neutral water and formaldehyde molecules, whereas different phosphate anions (PO_3^-, $H_2PO_3^-$ and PO^-, respectively) are excised from phosphodiesters [137]. The reactivity of these compounds at very low energy is consistent with the previously observed single strand breaks in plasmid DNA, which are generated with basically no threshold energy [156]. At higher energies between 1 and 3 eV, where the second maximum of the strand break yield was determined [123], the phosphate group is active towards low energy electrons [137]. In dibutylphosphate (DBP) a cleavage of a C–O bond was observed at 2–4 eV resulting in the abstraction of a butyl group[137]:

$$e^-(2\text{–}4\,\text{eV}) + PO_4(C_4H_9)_2 \rightarrow PO_4(C_4H_9)_2^{-\#} \rightarrow PO_4C_4H_9^- + C_4H_9 \quad (23)$$

Compared to the situation in DNA such a reaction would correspond to a direct strand break. Hence, low energy electron attachment to the individual DNA components shows that DEA, that eventually may lead to strand breaks, can occur at the nucleobases as well as the sugar unit and the phosphate group. However it is also obvious from these experiments that gas phase experiments on the larger units, i.e., individual nucleosides and the nucleotides as well as shorter oligonucleotides would be very valuable in our search to understand the role of low energy electrons in DNA damage by high energy radiation.

3.3.4. New experimental approaches to study electron attachment to biomolecular systems

To date the intrinsic properties of single DNA building blocks are well studied. However, it is still an open question, how an excess charge evolves that is located at a particular part of the DNA. Furthermore the contributions of different reaction pathways that are suggested by experiment and theory remain to be evaluated on larger systems. For this it is necessary to study more complex subunits of DNA, such as nucleosides, nucleotides and oligomers. However, the gas phase experiments on DEA of biomolecules that have been performed up to now employed thermal evaporation of the respective molecules. This sets a limit to the size and the nature of the molecules that can be studied as most of the larger biologically relevant molecules decompose before thermal sublimation. Therefore new experimental techniques are required that ensure the transfer of intact and neutral biomolecules into the gas phase.

One approach is now developed in Eugens laboratory, that utilizes laser-induced acoustic desorption [157] combined with DEA (see Section 2.2) [51,52]. Preliminary experiments indicate that DEA to nucleosides, sugar-phosphates and nucleotides can be studied successfully by this method thus enabling a completely new scope of experiments.

To our knowledge thymidine is the largest building block of the DNA that has been studied by conventional methods with respect to DEA in the gas phase [152]. The parent ion after loss of hydrogen $[Td–H]^-$ could be detected in these experiments, but the most abundant fragment ion was $[T–H]^-$, i.e., the closed shell anion of the dehydrogenated thymine. The ion yield curve of this fragment shows a structured low energy contribution in the range from about 1–3 eV that is identical to the low energy contribution observed in electron attachment to the isolated thymine nucleobase. Moreover, this low energy contribution also shows pronounced temperature dependence, indicating that the signal is in fact the result of electron attachment to the thymine nucleobase rather than the nucleoside thymidine. Hence the thermal evaporation causes degradation of thymidine resulting in DEA spectra that are dominated by electron attachment to the nucleobase, which represents a thermal decomposition product. In addition to the low energy contribution the $[T–H]^-$ fragment is also observed in the range from 5.5 to 9 eV [152]. This contribution was not observed before and was thus assigned to DEA to non-decomposed thymidine. The $[T–H]^-$ ion yield from DEA to thymidine evaporated with LIAD, i.e., thymidine that has been desorbed intact by a non-thermal mechanism, does not show any signal at lower energy but exclusively at higher energy between 5.5 and 9 eV [51,52]. Hence it is clear that ion formation proceeds exclusively through the higher energy resonances between 5.5 and 9 eV and that no $[T–H]^-$ is formed from thymidine at lower energies. The comparison also shows the need for softer evaporation methods to study large biomolecules and the potential of LIAD in this field.

The bottom-up approach of gas phase experiments reveals the intrinsic properties of certain molecular systems, but underestimates the relevance of an environment that is closer to a biological system. To address this question microarray techniques have been developed to study electron induced strand breaks in self-assembled monolayers of DNA [148,149]. Single DNA strands are immobilised on a gold surface and irradiated with electrons of defined energy. The formation of strand breaks upon electron irradiation is determined by hybridization of the remaining strands with the complementary strand, which is connected to a fluorescence dye. The decrease of fluorescence intensity compared to a non-irradiated sample on the same array is a measure of the loss of genetic information. Experiments on a dT_{25} DNA strand suggest that DNA damage occurs already at very low electron doses, i.e., a strand break occurs after exposure of the DNA strand to a few hundred electrons. Further experiments are in progress, in which the role of DNA binding proteins for radiation damage is investigated [142].

Acknowledgements

We acknowledge the previous and current members of Eugen Illenberger's research group for their valuable contributions that have made this review possible. We also appreciate the

contributions of our colleagues whose names appear in the articles that are cited in this review. Furthermore we would like to express our special thanks to Michael Allan and Petra Swiderek for instructive discussions during the preparation of the manuscript.

Appendix A. Supplementary data

Supplementary data associated with this article can be found, in the online version, at doi:10.1016/j.ijms.2008.06.013.

References

[1] L.G. Christophorou (Ed.), Electron–Molecule Interaction and Their Applications, Academic Press, Orlando, 1984.
[2] E. Illenberger, J. Momigny, Gaseous Molecular Ions, An Introduction to Elementary Processes Induced by Ionization, Steinkopf Verlag, Darmstadt/Springer–Verlag, New York, 1992.
[3] O. Ingólfsson, F. Weik, E. Illenberger, Int. J. Mass Spectrom. 155 (1996) 1.
[4] G.J. Schulz, Rev. Mod. Phys. 45 (1973) 423.
[5] M. Allan, J. Electron Spectrosc. Relat. Phenom. 48 (1989) 219.
[6] K. Raghavachari, R.C. Haddon, T.A. Miller, V.E. Bondybey, J. Chem. Phys. 79 (1983) 1387.
[7] J. Eiding, R. Schneider, W. Domcke, H. Koppel, W. Vonniessen, Chem. Phys. Lett. 177 (1991) 345.
[8] O. Ingólfsson, E. Illenberger, Int. J. Mass Spectrom. 150 (1995) 79.
[9] H.P. Fenzlaff, E. Illenberger, Int. J. Mass Spectrom. 59 (1984) 185.
[10] M. Fenzlaff, R. Gerhard, E. Illenberger, J. Chem. Phys. 88 (1988) 149.
[11] H. Hotop, M.W. Ruf, M. Allan, I.I. Fabrikant, Adv. Atomic Mol. Opt. Phys. (2003) 85.
[12] A. Hadjiant, L.G. Christophorou, J.G. Carter, J. Chem. Soc., Faraday Trans. 69 (1973) 1691.
[13] A.C. Sergenton, L. Jungo, M. Allan, Phys. Rev. A 6106 (2000).
[14] C. Desfrancois, H. Abdoul-Carime, C. Adjouri, N. Khelifa, J.P. Schermann, Europhys. Lett. 26 (1994) 25.
[15] R. Hashemi, E. Illenberger, J. Phys. Chem. 95 (1991) 6402.
[16] C. Desfrancois, H. Abdoulcarime, N. Khelifa, J.P. Schermann, Phys. Rev. Lett. 73 (1994) 2436.
[17] M. Allan, T. Skalicky, J. Phys. B: At. Mol. Opt. Phys. 36 (2003) 3397.
[18] M. Stepanovic, Y. Pariat, M. Allan, J. Chem. Phys. 110 (1999) 11376.
[19] A.M. Scheer, K. Aflatooni, G.A. Gallup, P.D. Burrow, Phys. Rev. Lett. 92 (2004).
[20] W. E., Phys. Rev. 72 (1948) 1002.
[21] D. Field, S.L. Lunt, T.P. Ziesel, Acc. Chem. Res. 34 (2001) 291.
[22] T. Jaffke, E. Illenberger, M. Lezius, S. Matejcik, D. Smith, T.D. Märk, Chem. Phys. Lett. 226 (1994) 213.
[23] S. Matejcik, T.D. Märk, P. Spanel, D. Smith, T. Jaffke, E. Illenberger, J. Chem. Phys. 102 (1995) 2516.
[24] S. Barsotti, M.W. Ruf, H. Hotop, Phys. Rev. Lett. 89 (2002).
[25] M. Braun, M.W. Ruf, I.I. Fabrikant, H. Hotop, Phys. Rev. Lett. 99 (2007).
[26] C.E. Klots, Chem. Phys. Lett. 38 (1976) 61.
[27] E.W. Vogt, G.H. Wannier, Phys. Rev. 95 (1954) 1190.
[28] H.S.W. Massey, Negative Ions, Cambridge University Press, Cambridge, 1976.
[29] T.F. O'Malley, Phys. Rev. 150 (1966) 14.
[30] O. Ingólfsson, F. Weik, E. Illenberger, Int. Rev. Phys. Chem. 15 (1996) 133.
[31] E. Illenberger, Chem. Rev. 92 (1992) 1589.
[32] R. Balog, J. Langer, S. Gohlke, M. Stano, H. Abdoul-Carime, E. Illenberger, Int. J. Mass Spectrom. 233 (2004) 267.
[33] H. Haberland, K.H. Bowen, in: H. Haberland (Ed.), Springer Series in Chemical Physics, vol. 56, Springer–Verlag, Berlin, 1994.
[34] J. Jortner, N.R. Kestner (Eds.), Electrons in Fluids, Springer, Berlin, 1973.
[35] U. Landman, R.N. Barnett, C.L. Cleveland, D. Scharf, J. Jortner, Int. J. Quantum Chem. (1987) 573.
[36] U. Landman, R.N. Barnett, C.L. Cleveland, D. Scharf, J. Jortner, J. Phys. Chem. 91 (1987) 4890.
[37] C.E. Klots, Radiat. Phys. Chem. 20 (1982) 51.
[38] F. Weik, L. Sanche, O. Ingólfsson, E. Illenberger, J. Chem. Phys. 112 (2000) 9046.
[39] F. Weik, E. Illenberger, J. Chem. Phys. 103 (1995) 1406.
[40] P. Tegeder, F. Brüning, E. Illenberger, Chem. Phys. Lett. 310 (1999) 79.
[41] F. Weik, E. Illenberger, K. Nagesha, L. Sanche, J. Phys. Chem. B 102 (1998) 824.
[42] F. Weik, E. Illenberger, J. Chem. Phys. 109 (1998) 6079.
[43] M. Meinke, E. Illenberger, J. Phys. Chem. 98 (1994) 6601.
[44] P. Tegeder, E. Illenberger, Chem. Phys. Lett. 341 (2001) 401.
[45] T. Oster, A. Kuhn, E. Illenberger, Int. J. Mass Spectrom. 89 (1989) 1.
[46] E. Illenberger, H.U. Scheunemann, H. Baumgartel, Chem. Phys. 37 (1979) 21.
[47] A. Kuhn, E. Illenberger, J. Chem. Phys. 93 (1990) 357.
[48] T. Oster, O. Ingólfsson, M. Meinke, T. Jaffke, E. Illenberger, J. Chem. Phys. 99 (1993) 5141.
[49] A. Stamatovic, G.J. Schulz, Rev. Sci. Instrum. 41 (1970) 423.
[50] E. Illenberger, Chem. Phys. Lett. 80 (1981) 153.
[51] I. Bald, Ph.D. Thesis, Freie Universität Berlin, Berlin, 2007.
[52] I. Bald, I. Dabkowska, E. Illenberger, submitted for publication.
[53] B. Lindner, U. Seydel, Anal. Chem. 57 (1985) 895.
[54] B. Lindner, Int. J. Mass Spectrom. 103 (1991) 203.
[55] R.C. Shea, C.J. Petzold, J.A. Liu, H.I. Kenttamaa, Anal. Chem. 79 (2007) 1825.
[56] L.G. Christophorou, M.O. Pace (Eds.), Gaseous Dielectrics, Pergamon, New York, 1984.
[57] K.H. Becker, in: R.P.R. Hippler, S. Schmidt, M.K.H. Schoenbach (Eds.), Low Temperature Plasma Physics, Wiley-VCH, Berlin, 2001.
[58] M.H. Rees, Physics and Chemistry of the Upper Atmosphere, Cambridge University Press, Cambridge, 1989.
[59] L. Sanche, Eur. Phys. J. D 35 (2005) 367.
[60] I. Bald, E. Illenberger, O. Ingólfsson, Chem. Phys. Lett. 442 (2007) 270.
[61] P. Tegeder, L. Lehmann, O. Ingólfsson, E. Illenberger, Z. Phys. Chem. 195 (1996) 217.
[62] G.W. Dillow, P. Kebarle, J. Am. Chem. Soc. 111 (1989) 5592.
[63] J. Langer, I. Dabkowska, Y. Zhang, E. Illenberger, Phys. Chem. Chem. Phys. 10 (2008) 1523.
[64] I. Dabkowska, H.D. Flosadóttir, S. Ptasinska, I. Bald, O. Ingólfsson, E. Illenberger, submitted for publication.
[65] M.B. Robin, Higher Excited States of Polyatomic Molecules, Academic Press, New York, 1975.
[66] I. Hahndorf, E. Illenberger, Int. J. Mass Spectrom. 167 (1997) 87.
[67] E. Illenberger, in: N.C.Y. (Ed.), Photoionization and Photodetachment, World Scientific, Singapore, 2000.
[68] H. Drexel, W. Sailer, V. Grill, P. Scheier, E. Illenberger, T.D. Märk, J. Chem. Phys. 118 (2003) 7394.
[69] G. Herzberg, Spectra of Diatomic Molecules, Van Nostrand, New York, 1950.
[70] T.K. Ha, G. Zumofen, Mol. Phys. 40 (1980) 445.
[71] F. Brüning, I. Hahndorf, A. Stamatovic, E. Illenberger, J. Phys. Chem. 100 (1996) 19740.
[72] D. Spence, G.J. Schulz, J. Chem. Phys. 58 (1973) 1800.
[73] L. Lehr, W.H. Miller, Chem. Phys. Lett. 250 (1996) 515.
[74] A. Rosa, W. Barszczewska, D. Nandi, V. Ashok, S.V.K. Kumar, E. Krishnakumar, F. Brüning, E. Illenberger, Chem. Phys. Lett. 342 (2001) 536.
[75] I. Hahndorf, E. Illenberger, L. Lehr, J. Manz, Chem. Phys. Lett. 231 (1994) 460.
[76] S. Matejcik, I. Ipolyi, E. Illenberger, Chem. Phys. Lett. 375 (2003) 660.
[77] I. Ipolyi, S. Matejcik, E. Illenberger, Eur. Phys. J. D 35 (2005) 257.
[78] M. Heni, E. Illenberger, Chem. Phys. Lett. 131 (1986) 314.
[79] Y. Le Coat, R. Azria, M. Tronc, O. Ingólfsson, E. Illenberger, Chem. Phys. Lett. 296 (1998) 208.
[80] E.C.M. Chen, L.R. Shuie, E.D. Dsa, C.F. Batten, W.E. Wentworth, J. Chem. Phys. 88 (1988) 4711.
[81] T.M. Miller, A.E.S. Miller, J.F. Paulson, X.F. Liu, J. Chem. Phys. 100 (1994) 8841.
[82] D. Smith, P. Spanel, S. Matejcik, A. Stamatovic, T.D. Märk, T. Jaffke, E. Illenberger, Chem. Phys. Lett. 240 (1995) 481.
[83] L.G. Christophorou, J.K. Olthoff, Int. J. Mass Spectrom. 205 (2001) 27.
[84] M. Braun, S. Barsotti, S. Marienfeld, E. Leber, J.M. Weber, M.W. Ruf, H. Hotop, Eur. Phys. J. D 35 (2005) 177.
[85] I. Bald, I. Dabkowska, E. Illenberger, O. Ingólfsson, Phys. Chem. Chem. Phys. 9 (2007) 2983.
[86] F.M. Zimmermann, W. Ho, Surf. Sci. Rep. 22 (1995) 127.
[87] R. Naaman, L. Sanche, Chem. Rev. 107 (2007) 1553.
[88] B. Boudaiffa, P. Cloutier, D. Hunting, M.A. Huels, L. Sanche, Science 287 (2000) 1658.
[89] P.A. Sloan, R.E. Palmer, Nature 434 (2005) 367.
[90] S.W. Hla, K.H. Rieder, Annu. Rev. Phys. Chem. 54 (2003) 307.
[91] J.I. Pascual, N. Lorente, Z. Song, H. Conrad, H.P. Rust, Nature 423 (2003) 525.
[92] P. Tegeder, B.M. Smirnov, E. Illenberger, Int. J. Mass Spectrom. 205 (2001) 331.
[93] F. Brüning, P. Tegeder, J. Langer, E. Illenberger, Int. J. Mass Spectrom. 196 (2000) 507.
[94] E. Illenberger, Surf. Sci. 528 (2003) 67.
[95] P. Tegeder, E. Illenberger, Chem. Phys. Lett. 411 (2005) 175.
[96] P. Rowntree, L. Parenteau, L. Sanche, J. Phys. Chem. 95 (1991) 523.
[97] R. Hashemi, E. Illenberger, Chem. Phys. Lett. 187 (1991) 623.
[98] R. Hashemi, T. Jaffke, L.G. Christophorou, E. Illenberger, J. Phys. Chem. 96 (1992) 10605.
[99] T. Jaffke, R. Hashemi, L.G. Christophorou, E. Illenberger, Z. Phys. D 25 (1992) 77.
[100] A. Kuhn, E. Illenberger, J. Phys. Chem. 93 (1989) 7060.
[101] J. Langer, M. Stano, S. Gohke, A. Rosa, W. Barszczewska, S. Matejcík, E. Illenberger, Int. J. Mass Spectrom. 223 (2003) 193.
[102] J. Langer, S. Matejcik, E. Illenberger, Int. J. Mass Spectrom. 220 (2002) 211.
[103] M.J. Travers, D.C. Cowles, G.B. Ellison, Chem. Phys. Lett. 164 (1989) 449.
[104] Y. Chu, G. Senn, S. Matejcik, P. Scheier, P. Stampfli, A. Stamatovic, E. Illenberger, T.D. Märk, Chem. Phys. Lett. 289 (1998) 521.
[105] S. Matejcik, A. Kiendler, P. Stampfli, A. Stamatovic, T.D. Märk, Phys. Rev. Lett. 77 (1996) 3771.
[106] P. Rowntree, H. Sambe, L. Parenteau, L. Sanche, Phys. Rev. B 47 (1993) 4537.
[107] P. Rowntree, L. Parenteau, L. Sanche, Chem. Phys. Lett. 182 (1991) 479.
[108] J. Langer, S. Matt, M. Meinke, P. Tegeder, A. Stamatovic, E. Illenberger, J. Chem. Phys. 113 (2000) 11063.
[109] P. Tegeder, E. Illenberger, Phys. Chem. Chem. Phys. 1 (1999) 5197.
[110] N. Ruckhaberle, L. Lehmann, S. Matejcik, E. Illenberger, Y. Bouteiller, V. Periquet, L. Museur, C. Desfrancois, J.P. Schermann, J. Phys. Chem. A 101 (1997) 9942.
[111] A. Lafosse, M. Bertin, A. Domaracka, D. Pliszka, E. Illenberger, R. Azria, Phys. Chem. Chem. Phys. 8 (2006) 5564.

[112] I. Ipolyi, W. Michaelis, P. Swiderek, Phys. Chem. Chem. Phys. 9 (2007) 180.
[113] A. Lafosse, M. Bertin, D. Caceres, C. Jaggle, P. Swiderek, D. Pliszka, R. Azria, Eur. Phys. J. D 35 (2005) 363.
[114] H. Winterling, H. Haberkern, P. Swiderek, Phys. Chem. Chem. Phys. 3 (2001) 4592.
[115] R. Balog, M.N. Hedhili, F. Bournel, M. Penno, M. Tronc, R. Azria, E. Illenberger, Phys. Chem. Chem. Phys. 4 (2002) 3350.
[116] R. Balog, E. Illenberger, Phys. Rev. Lett. 91 (2003).
[117] T. Sedlacko, R. Balog, A. Lafosse, M. Stano, S. Matejcik, R. Azria, E. Illenberger, Phys. Chem. Chem. Phys. 7 (2005) 1277.
[118] M. Orzol, T. Sedlacko, R. Balog, J. Langer, G.P. Karwasz, E. Illenberger, A. Lafosse, M. Bertin, A. Domaracka, R. Azria, Int. J. Mass Spectrom. 254 (2006) 63.
[119] L. Lehmann, S. Matejcik, E. Illenberger, Ber. Buns. Ges. Phys. Chem. Chem. Phys. 101 (1997) 287.
[120] L. Lehmann, E. Illenberger, Int. J. Mass Spectrom. 187 (1999) 463.
[121] J. Langer, S. Matejcik, E. Illenberger, Phys. Chem. Chem. Phys. 2 (2000) 1001.
[122] J. Langer, I. Martin, G. Karwasz, E. Illenberger, Int. J. Mass Spectrom. 249 (2006) 477.
[123] F. Martin, P.D. Burrow, Z.L. Cai, P. Cloutier, D. Hunting, L. Sanche, Phys. Rev. Lett. 93 (2004).
[124] M.A. Huels, I. Hahndorf, E. Illenberger, L. Sanche, J. Chem. Phys. 108 (1998) 1309.
[125] H. Abdoul-Carime, S. Gohlke, E. Illenberger, Phys. Rev. Lett. 92 (2004).
[126] S. Ptasinska, S. Denifl, V. Grill, T.D. Märk, P. Scheier, S. Gohlke, M.A. Huels, E. Illenberger, Angew. Chem. Int. Ed. 44 (2005) 1647.
[127] K. Aflatooni, A.M. Scheer, P.D. Burrow, Chem. Phys. Lett. 408 (2005) 426.
[128] A.M. Scheer, C. Silvernail, J.A. Belot, K. Aflatooni, G.A. Gallup, P.D. Burrow, Chem. Phys. Lett. 411 (2005) 46.
[129] H. Abdoul-Carime, J. Langer, M.A. Huels, E. Illenberger, Eur. Phys. J. D 35 (2005) 399.
[130] S. Ptasinska, S. Denifl, P. Scheier, E. Illenberger, T.D. Märk, Angew. Chem. Int. Ed. 44 (2005) 6941.
[131] P.D. Burrow, G.A. Gallup, A.M. Scheer, S. Denifl, S. Ptasinska, T.D. Märk, P. Scheier, J. Chem. Phys. 124 (2006).
[132] R. Abouaf, J. Pommier, H. Dunet, Int. J. Mass Spectrom. 226 (2003) 397.
[133] S. Ptasinska, S. Denifl, V. Grill, T.D. Märk, E. Illenberger, P. Scheier, Phys. Rev. Lett. 95 (2005).
[134] I. Baccarelli, F.A. Gianturco, A. Grandi, N. Sanna, R.R. Lucchese, I. Bald, J. Kopyra, E. Illenberger, J. Am. Chem. Soc. 129 (2007) 6269.
[135] I. Bald, J. Kopyra, E. Illenberger, Angew. Chem. Int. Ed. 45 (2006) 4851.
[136] S. Denifl, S. Matejcik, S. Ptasinska, B. Gstir, M. Probst, P. Scheier, E. Illenberger, T.D. Märk, J. Chem. Phys. 120 (2004) 704.
[137] C. König, J. Kopyra, I. Bald, E. Illenberger, Phys. Rev. Lett. 97 (2006).
[138] H.D. Flosadóttir, S. Denifl, F. Zappa, N. Wendt, A. Mauracher, A. Bacher, H. Jonsson, T.D. Märk, P. Scheier, O. Ingólfsson, Angew. Chem. Int. Ed. 46 (2007) 8057.
[139] A. Mauracher, S. Denifl, A. Aleem, N. Wendt, F. Zappa, P. Cicman, M. Probst, T.D. Märk, P. Scheier, H.D. Flosadottir, O. Ingólfsson, E. Illenberger, Phys. Chem. Chem. Phys. 9 (2007) 5680.
[140] Y.V. Vasil'ev, B.J. Figard, V.G. Voinov, D.F. Barofsky, M.L. Deinzer, J. Am. Chem. Soc. 128 (2006) 5506.
[141] S. Ptasinska, S. Denifl, P. Candori, S. Matejcik, P. Scheier, T.D. Märk, Chem. Phys. Lett. 403 (2005) 107.
[142] H. Abdoul-Carime, E. Illenberger, Chem. Phys. Lett. 397 (2004) 309.
[143] H. Abdoul-Carime, S. Gohlke, E. Illenberger, Phys. Chem. Chem. Phys. 6 (2004) 161.
[144] H. Abdoul-Carime, S. Gohlke, E. Illenberger, Chem. Phys. Lett. 402 (2005) 497.
[145] K. Aflatooni, B. Hitt, G.A. Gallup, F.D. Burrow, J. Chem. Phys. 115 (2001) 6489.
[146] P. Papp, J. Urban, S. Matejcik, M. Stano, O. Ingólfsson, J. Chem. Phys. 125 (2006).
[147] S. Gohlke, A. Rosa, E. Illenberger, F. Brüning, M.A. Huels, J. Chem. Phys. 116 (2002) 10164.
[148] T. Solomun, C. Hultschig, E. Illenberger, Eur. Phys. J. D 35 (2005) 437.
[149] T. Solomun, E. Illenberger, Chem. Phys. Lett. 396 (2004) 448.
[150] S. Ptasinska, S. Denifl, A. Abedi, P. Scheier, T.D. Märk, Anal. Bioanal. Chem. 377 (2003) 1115.
[151] J. Simons, Acc. Chem. Res. 39 (2006) 772.
[152] S. Ptasinska, S. Denifl, S. Gohlke, P. Scheier, E. Illenberger, T.D. Märk, Angew. Chem. Int. Ed. 45 (2006) 1893.
[153] H. Abdoul-Carime, S. Gohlke, E. Fischbach, J. Scheike, E. Illenberger, Chem. Phys. Lett. 387 (2004) 267.
[154] P. Sulzer, S. Ptasinska, F. Zappa, B. Mielewska, A.R. Milosavljevic, P. Scheier, T.D. Märk, I. Bald, S. Gohlke, M.A. Huels, E. Illenberger, J. Chem. Phys. 125 (2006).
[155] I. Bald, J. Kopyra, I. Dabkowska, E. Antonsson, E. Illenberger, J. Chem. Phys. 126 (2007).
[156] R. Panajotovic, F. Martin, P. Cloutier, D. Hunting, L. Sanche, Radiat. Res. 165 (2006) 452.
[157] R.C. Shea, C.J. Petzold, J.L. Campbell, S. Li, D.J. Aaserud, H.I. Kenttamaa, Anal. Chem. 78 (2006) 6133.
[158] K.E. Crawford, J.L. Campbell, M.N. Fiddler, P. Duan, K. Qian, M.L. Gorbaty, H.I. Kenttamaa, Anal. Chem. 77 (2005) 7916.